

# The Equilibrium Hypothesis: Rethinking implicit regularization in Deep Neural Networks

**Yizhang Lou**

*St. John's College  
University of Oxford  
Oxford, UK*

YIZHANG.LOU@SJC.OX.AC.UK

**Chris Mingard**

*Department of Chemistry  
University of Oxford  
Oxford, UK*

CHRISTOPHER.MINGARD@CHEM.OX.AC.UK

**Soufiane Hayou**

*Department of Mathematics  
National University of Singapore  
Singapore*

HAYOU@NUS.EDU.SG

## Abstract

Modern Deep Neural Networks (DNNs) exhibit impressive generalization properties on a variety of tasks without explicit regularization, suggesting the existence of hidden regularization effects. Recent work by [Baratin et al. \(2021\)](#) sheds light on an intriguing implicit regularization effect, showing that some layers are much more *aligned* with data labels than other layers. This suggests that as the network grows in depth and width, an implicit *layer selection* phenomenon occurs during training. In this work, we provide the first explanation for this *alignment hierarchy*. We introduce and empirically validate the *Equilibrium Hypothesis* which states that the layers that achieve some balance between forward and backward information loss are the ones with the highest alignment to data labels. Our experiments demonstrate an excellent match with the theoretical predictions.

## 1. Introduction

Although modern Deep Neural Networks (DNNs) are massively overparameterized, they still achieve impressive generalization error without additional regularization techniques [Zhang et al. \(2021\)](#). To understand the reasons behind this unexpected behaviour, a stream of research papers studied different regularization effects that occur during DNNs training.

**Regularization.** The performance-enhancing effect of avoiding over-fitting by regularization is well-established in statistical theory. Classical techniques include adding penalty terms to the loss function (e.g.  $L_1, L_2$  penalties); these methods are often called *explicit* regularization techniques as they act directly on the loss function. There is an extensive literature on explicit regularization in DNNs, especially on noise-based regularization techniques, to cite a few; Dropout ([Hinton et al., 2012](#); [Wager et al., 2013](#); [Mianjy and Arora, 2019](#); [Cavazza et al., 2017](#); [Wei et al., 2020](#)), Stochastic Depth ([Huang et al., 2016](#); [Hayou and Ayed, 2021](#)), Gaussian-noise injection [Camuto et al. \(2020\)](#). On the other hand, *implicit* regularization refers to any hidden regularization effect induced by the training algorithm, e.g. the regularizing effect of the noise in Stochastic Gradient Descent (SGD).

**Implicit regularization.** SGD (Lecun et al., 1998) has become the algorithm of choice in training deep neural networks (see e.g. He et al. (2015); Krizhevsky et al. (2012)). It is widely believed that SGD is an implicit regularizer, mainly driven by the small-batch sampling noise (Jastrzebski et al., 2018), which acts as a noise-based regularization method. Recent empirical findings such as (Wu et al., 2017; Geiping et al., 2021) demonstrated that DNNs can still achieve high accuracy on some image datasets with full-batch GD. Goyal et al. (2017) demonstrated that increasing batch size by several orders of magnitude on ImageNet does not affect generalization error significantly, suggesting that classical implicit regularization theories that rely on SGD noise to explain generalization are not sufficient to explain why neural networks generalize *at all*. Furthermore, Wu et al. (2020) showed that other types of noise regularizes equally effectively as that in SGD. These results suggest that implicit regularization might have different mechanisms than previously thought. Indeed, recent work by Baratin et al. (2021) demonstrated the existence of a layer hierarchy in which some layers are more effectively trained compared to others, suggesting the existence of a *structural* implicit regularization effect that favors some layers over the others during training. To explain these findings, we introduce the Equilibrium Hypothesis which conjectures that this effect is a result of a notion of balance between forward and backward information propagation at initialization.

**The Equilibrium Hypothesis (EH)** (*Informal*). *The layers that achieve a balance between forward and backward information flow at initialization have the largest alignment with data labels.*

## 1.1 Our contributions

Our contributions are three-fold. Firstly, we introduce and empirically validate the EH on a variety of vision tasks. Secondly, we provide a comprehensive analysis of the EH in the case of fully-connected neural networks. Most notably, we prove that layers with indices  $\mathbf{l} = \Theta(\mathbf{L}^{3/5})$  achieve an *equilibrium* between forward and backward information flow in the limit of large depth  $L$ . Our experiments yield excellent match between theoretical and empirical results. Finally, we connect the EH to early training steps, showing why information balance results in more effective training.

## 2. Tangent Features and Alignment

Consider a neural network model consisting of  $L$  layers of widths  $(N_l)_{1 \leq l \leq L}$ ,  $N_0 = d$ , and let  $\theta = (\theta_l)_{1 \leq l \leq L}$  be the flattened vector of weights indexed by the layer’s index, and  $P$  be the dimension of  $\theta$ . Given an input  $x \in \mathbb{R}^d$ , the network is described by the set of equations

$$z_l(x) = \mathcal{F}_l(\theta_l, z_{l-1}(x)), \quad 1 \leq l \leq L,$$

where  $\mathcal{F}_l$  is a mapping that defines the  $l^{\text{th}}$  layer, e.g. fully-connected, convolutional, etc. The network output function  $f$  is given by  $f_\theta(x) = \nu(z_L(x)) \in \mathbb{R}^o$  where  $\nu : \mathbb{R}^{N_L} \rightarrow \mathbb{R}^o$  is a mapping of choice, and  $o$  is the dimension of the output, e.g. the number of classes for a classification problem.

We consider a loss function  $\mathbb{L} : \mathbb{R}^o \times \mathbb{R}^o \rightarrow \mathbb{R}$  and a dataset  $\mathcal{D} = \{(x_1, y_1), \dots, (x_n, y_n)\}$ . The

network is then trained by minimizing the empirical loss  $\mathcal{L} : \mathbb{R}^P \rightarrow \mathbb{R}$  given by

$$\mathcal{L}(\theta) = \frac{1}{n} \sum_{i=1}^n \mathbb{L}(f_\theta(x_i), y_i).$$

**Tangent Features.** Jacot et al. (2018) introduced the Neural Tangent Kernel (NTK), which provides a dual view of the training procedure; it links gradient updates in parameter space to a kernel gradient descent in function space. The NTK is given by

$$\begin{aligned} \mathbf{K}_\theta^L(x, x') &= \nabla_\theta f_\theta(x) \nabla_\theta f_\theta(x')^T \\ &= \sum_{l=1}^L \nabla_{\theta_l} f_\theta(x) \nabla_{\theta_l} f_\theta(x')^T \in \mathbb{R}^{o \times o}. \end{aligned} \tag{1}$$

The tangent features are the feature maps of the NTK, given by the output gradients w.r.t the network parameters, namely

$$\Psi_\theta(x) := \nabla_\theta f_\theta(x)^T \in \mathbb{R}^{P \times o}. \tag{2}$$

For the sake of simplicity, we remove  $\theta$  and  $L$  in the kernel notation and define  $\Psi \in \mathbb{R}^{P \times on}$ , the tangent feature matrix over the training dataset  $\mathcal{D}$ .  $\Psi$  is the horizontal concatenation of  $\Psi(x_1), \dots, \Psi(x_n)$ . The corresponding tangent kernel matrix is given by  $\mathbf{K} = \Psi^T \Psi \in \mathbb{R}^{on \times on}$ .

**Why do tangent features matter in DNN training?** Let  $f_t$  be the output function at training time  $t$ , and  $X$ , resp.  $Y$ , be the concatenated matrix of inputs, resp. outputs. Lee et al. (2019a) showed that with gradient flow dynamics, for some  $x \in \mathbb{R}^d$ ,  $df_t(x) = -\mathbf{K}_\theta^L(x, X) \nabla_y \mathbb{L}(f_t(X), Y) dt$ , where  $\mathbb{L}(f_t(X), Y)$  is the flattened vector of loss gradients. Therefore, the infinitesimal changes in  $f_t$  are controlled by the tangent features, i.e.  $df_t$  lives in the Reproducing Kernel Hilbert Space of the NTK. Hence, understanding how tangent features evolve during training might provide valuable insights on DNNs generalization properties.

**Feature learning.** Lee et al. (2020, 2019b); Valle-Perez et al. (2018); Mingard et al. (2021) demonstrated that neural network based kernel methods (e.g. infinite width NTK regime) can achieve parity with finite width networks, and have near identical posterior distributions, over a range of architectures (e.g. LSTMs, WideResNet) and datasets (e.g. Cifar10). However, optimizer hyperparameters are known to affect generalization, suggesting an extra layer of complexity (Bernstein and Yue, 2021; Mingard et al., 2021). Furthermore, Hayou et al. (2020) proved that the large depth limit of the NTK regime is trivial in the sense that the limiting NTK has rank 1. This suggests that this kernel regime, where tangent features are fixed at initialization, cannot explain the inductive bias of ultra deep neural networks, and that feature learning (tangent features evolve during training) could be the backbone of generalization in very deep networks. Recent work by Baratin et al. (2021) studied this change in the NTK using a measure of the alignment of the tangent features with data labels (for classification tasks) which we introduce in the next paragraph.

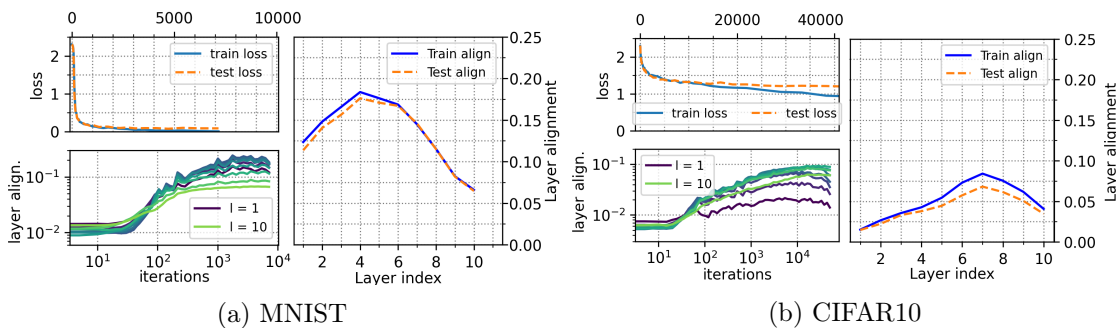


Figure 1: Layerwise alignment hierarchy for the MNIST and CIFAR10 datasets when trained on an FFNN with depth 10 and width 256. Left hand panels show progression of loss and layer alignment with iterations of SGD. Right hand panel shows layer alignment at the end of training.

**Centered Kernel Alignment (CKA).** Following Baratin et al. (2021), the *centered kernel alignment* between two kernel matrices  $\mathbf{K}, \mathbf{K}' \in \mathbb{R}^{on \times on}$  is defined by

$$A(\mathbf{K}, \mathbf{K}') = \frac{\text{Tr}[\mathbf{K}_c \mathbf{K}'_c]}{\|\mathbf{K}_c\|_F \|\mathbf{K}'_c\|_F} \quad (3)$$

where  $\mathbf{K}_c = \mathbf{C}\mathbf{K}\mathbf{C}$ ,  $\mathbf{C} = \mathbf{I} - \frac{1}{on}\mathbf{1}\mathbf{1}^T$  is the centering matrix ( $\mathbf{1}$  is a vector with all entries being 1), and  $\|\cdot\|_F$  is the Frobenius norm.

*Remark 1.* For all kernels  $\mathbf{K}, \mathbf{K}'$ , we have  $A(\mathbf{K}, \mathbf{K}') \in [0, 1]$  with  $A(\mathbf{K}, \mathbf{K}') = 1$  if and only if the kernel matrices are colinear.

To measure the alignment of the tangent features with data, we use  $\mathbf{K} = \Psi^T \Psi$ , the tangent kernel matrix defined above, and  $\mathbf{K}' = \mathbf{Y}\mathbf{Y}^T$  where  $\mathbf{Y} \in \mathbb{R}^{on}$  is the horizontal concatenation of output vectors in the dataset  $\mathcal{D}$ . Let  $\mathbf{y} = \mathbf{C}\mathbf{Y}$  be the centered labels. Using the relation  $\mathbf{C}^2 = \mathbf{C}$ , the CKA is given by

$$A(\mathbf{K}, \mathbf{K}') = \frac{\mathbf{y}^T \Psi^T \Psi \mathbf{y}}{\|\mathbf{C}\Psi^T \Psi \mathbf{C}\|_F \|\mathbf{y}\|^2} \quad (4)$$

**Layer CKA.** The NTK kernel can be decomposed into a sum of layerwise tangent kernels as shown in Eq. (1). We can therefore define the layerwise version of CKA by

$$A_l := A(\mathbf{K}_l, \mathbf{K}'_l) = \frac{\mathbf{y}^T \Psi_l^T \Psi_l \mathbf{y}}{\|\mathbf{C}\Psi_l^T \Psi_l \mathbf{C}\|_F \|\mathbf{y}\|^2} \quad (5)$$

where  $\Psi_l \in \mathbb{R}^{P_l \times on}$  is the horizontal concatenation of the tangent features ( $\Psi_l(x_i) = \nabla_{\theta_l} f_{\theta}(x_i)_{1 \leq i \leq n}$ , and  $P_l$  is the dimension of  $\theta_l$ ).

**Alignment Hierarchy.** Baratin et al. (2021) observed an interesting hierarchical structure in layer CKA alignments  $A_l$  for different neural network architectures. During the course of training, the increase in layer CKA of some middle layers is sharp and significantly larger than the alignments of other layers. Fig. 1 illustrates this pattern on MNIST and CIFAR10 datasets. It appears that some layers are trained<sup>1</sup> much more effectively than

1. In the sense they adapt much more to the data as measured by the CKA.

others, suggesting the existence of an implicit layer selection phenomenon during training. We call this pattern the *Alignment Hierarchy*, and aim to understand its cause. For both datasets, the pattern is similar and shows large alignments for some middle layers. Further empirical results on K-MNIST and FashionMNIST datasets and VGG19/ResNet18 architectures are provided in Appendix D. Motivated by this empirical findings, we formulate the Equilibrium Hypothesis in the next section, which connects the Alignment Hierarchy to a precise notion of balance between forward and backward information flows at initialization. We conjecture that the layers with a good balance are better conditioned to align with the data. In Fig. 4b, we show that high alignments generally correlate with better generalization.

### 3. The Equilibrium Hypothesis

We argue that the Alignment Hierarchy is a result of the dynamics that control signal propagation in DNNs. To formalize our intuition, we restrict our theoretical analysis to fully-connected DNNs, although our results can in principle be extended to other architectures.

**Fully-connected Feedforward Neural Network (FFNN).** Given an input  $x \in \mathbb{R}^d$ , and a set of weights and bias  $(W_l)_{1 \leq L}$ , we consider the following neural network model

$$\begin{aligned} z_1(x) &= W_1 x \\ z_l(x) &= W_l \phi(z_{l-1}(x)), \quad 2 \leq l \leq L, \end{aligned} \tag{6}$$

where  $W_l \in \mathbb{R}^{N_l \times N_{l-1}}$  with  $o = N_L = 1^2$ , and  $\phi$  is the ReLU activation function given by  $\phi(v) = (\max(v_i, 0))_{1 \leq i \leq p}$  for  $v \in \mathbb{R}^p$ . For each layer, the weights are initialized with i.i.d Gaussian variables  $W_l^{ij} \sim \mathcal{N}(0, \frac{2}{N_{l-1}})$ . This initialization scheme is known as the He initialization (He et al., 2015) or the Edge of Chaos initialisation (Poole et al., 2016; Schoenholz et al., 2017; Hayou et al., 2019).

**Tangent Kernel decomposition.** The tangent kernel at layer  $l$  can be decomposed as follows

$$\begin{aligned} K_l(x, x') &= \frac{\partial f}{\partial \theta_l}(x) \cdot \frac{\partial f}{\partial \theta_l}(x') \\ &= \sum_{i,j} \phi(z_{l-1}^j(x)) \phi(z_{l-1}^j(x')) \frac{\partial f}{\partial z_l^i}(x) \frac{\partial f}{\partial z_l^i}(x') \end{aligned}$$

Since  $K_l$  is a sum over  $N_l \times N_{l-1}$  terms, we consider the average kernel  $\bar{K}_l$  given by  $\bar{K}_l = \frac{1}{N_l N_{l-1}} K_l$ . In matrix form,  $\bar{K}_l$  can be written as the Hadamard product of two kernels

$$\bar{K}_l = \vec{K}_l \circ \overleftarrow{K}_l \tag{7}$$

where  $\vec{K}_l(x, x') = \frac{1}{N_{l-1}} \phi(z_{l-1}(x)) \cdot \phi(z_{l-1}(x'))$  is the *forward* features kernel and  $\overleftarrow{K}_l(x, x') = \frac{1}{N_l} \frac{\partial f_{l:L}}{\partial z}(z_l(x)) \cdot \frac{\partial f_{l:L}}{\partial z}(z_l(x'))$  is the *backward* tangent features kernel, where  $f_{l:L}$  is the function that maps the  $l^{\text{th}}$  layer to the network output. The above decomposition illustrates the

---

2. For simplicity, we restrict our analysis to 1D output networks. The generalization to  $o \in \mathbb{N}$  is straightforward.

collaborative roles played by kernels  $\overrightarrow{K}$  and  $\overleftarrow{K}$  in constructing the tangent features at layer  $l$ . To depict the role of each kernel, we first present a brief summary of the theory of signal propagation at initialization.

**Signal propagation at initialization.** Consider an FFNN of type (6). Since the weights at the first layer are i.i.d, neurons  $\{z_1^i(\cdot)\}_{i \in [1:N_1]}$  are also iid Gaussian processes with covariance kernel given by  $\mathbb{E}_W[z_1^i(x)z_1^i(x')] = \frac{2x \cdot x'}{d}$ . Using the Central Limit Theorem, as  $N_1 \rightarrow \infty$ ,  $z_1^i(x)$  is a Gaussian variable for any input  $x$  and index  $i \in [1 : N_2]$ . Moreover, the variables  $\{z_2^i(x)\}_{i \in [1:N_2]}$  are iid. Hence, the processes  $z_2^i(\cdot)$  can be seen as independent (across  $i$ ), centered Gaussian processes with some covariance kernel  $q_2$ . Doing this recursively over  $l$  leads to similar approximations for  $z_l^i(\cdot)$  where  $l \in [1 : L]$ . The approximation of  $z_l^i(\cdot)$  by a Gaussian process was first proposed by Neal (1995) in the single layer case and was extended to multi-layer networks by Lee et al. (2018) and Matthews et al. (2018). This result was also proven for almost all neural network architectures (Yang, 2019b). The covariance kernel  $q_l$  corresponding to  $z_l^1(\cdot)$  represents the forward information, while a similar kernel can be defined for the backward information (see Appendix A.3).

**Definition 1.** Given two inputs  $x, x' \in \mathbb{R}^d$ , we call the forward information  $I_f^l(x, x')$  for layer  $l$  the following quantity

$$I_f^l(x, x') = \mathbb{E}_W \left[ \overrightarrow{K}_l(x, x') \right] = \mathbb{E}_W \left[ \phi(z_{l-1}^1(x))\phi(z_{l-1}^1(x')) \right],$$

where the expectation is taken w.r.t random weights  $W$ . Note that the choice of the index 1 is not important since vectors  $(z_l^i(x), z_l^i(x'))_{1 \leq i \leq N_l}$  are identically distributed. Similarly, we define the backward information  $I_b^l(x, x')$  for layer  $l$  by

$$I_b^l(x, x') = \mathbb{E}_W \left[ \overleftarrow{K}_l(x, x') \right] = \mathbb{E}_W \left[ \frac{\partial f_{l:L}}{\partial z^1}(z_l(x)) \frac{\partial f_{l:L}}{\partial z^1}(z_l(x')) \right].$$

As the network depth  $L$  grows, we would expect some kind of deterioration of the forward/backward information. We formalize this idea in the next definition.

**Definition 2** (Information Loss Rate (ILR)). Let  $(g_n(\cdot))_{n \geq 0}$  be a sequence of real-valued functions defined on some set  $E \in \mathbb{R}^d$ . Assume that  $g_n$  converges uniformly to some constant  $\kappa$  as  $n \rightarrow \infty$  and that there exists a non-negative sequence  $(r_n)_{n \geq 0}$  such that  $\sup_{x \in E} |g_n(x) - \kappa| = \Theta(r_n)$ . We say that  $g_n$  has an information loss rate of  $r_n$ .

The ILR characterizes the rate at which the sequence  $(g_n(x))_{n \geq 1}$  forgets the information carried by the input  $x$  since, by definition, the limiting value  $\kappa$  is independent of  $x$ . We now use the ILR to present the Equilibrium Hypothesis.

**The Equilibrium Hypothesis (EH).** Let  $\text{ILR}_f^l$ , resp.  $\text{ILR}_b^l$ , be the information loss rate of the sequence  $(I_f^l)_{l \geq 1}$ , resp.  $(I_b^l)_{l \geq 1}$ . The layers with the highest alignments with data labels are the ones that satisfy the equilibrium property

$$\text{ILR}_f^l = \Theta \left( \text{ILR}_b^l \right).$$

The EH conjectures that balanced information flow between forward and backward propagation is related to high alignment with data. This entails that *feature learning* is more

effective<sup>3</sup> in the layers that satisfy this balance property.

For FFNNs, we provide a comprehensive analysis of the EH which allows us to characterize the layers where the equilibrium is achieved. Empirical results confirm our theoretical findings. For the sake of simplicity, we restrict our theoretical analysis to the sphere  $\sqrt{d}\mathbb{S}^d = \{x \in \mathbb{R}^d, \|x\| = \sqrt{d}\}$  where  $\|\cdot\|$  is the euclidean norm. The generalization to  $\mathbb{R}^d$  is straightforward.

**Assumption 1.** For all  $(x, y) \in \mathcal{D}$ ,  $\|x\| = \sqrt{d}$ .

To avoid dealing with different notions of infinite width, we focus on the case of rectangular networks, i.e. layer widths are the same.

**Assumption 2.** The widths are given by  $N_l = N$  for  $1 \leq l \leq L - 1$  where  $N$  is some integer. When  $N \rightarrow \infty$ , the widths  $N_l$ 's grow at the same rate.

It turns out that we can exactly characterize the ILR of the forward/backward information defined above. In the next result, we prove that the sequence  $(I_f^l(\cdot, \cdot))_{l \geq 1}$  has an ILR of  $l^{-2}$ .

**Theorem 3** (Forward ILR). Let  $\epsilon \in (0, 1)$ , and define  $E_\epsilon = \{(x, x') \in (\sqrt{d}\mathbb{S}^d)^2 : \frac{1}{d}x \cdot x' < 1 - \epsilon\}$ . Under Assumption 1, in the infinite width limit, we have that

$$\sup_{(x, x') \in E_\epsilon} |I_f^l(x, x') - 1/2| = \Theta(l^{-2})$$

Theorem 3 is a corollary of a previous result that appeared in Hayou et al. (2020). The proof of the latter relies on an asymptotic analysis of the forward covariance kernel in the limit of large  $l$ , coupled with a uniform bounding of the convergence rate (See Appendix B for more details).

Unlike the forward information  $I_f^l$  that depends only on the layer index  $l$ , the backward information  $I_b^l$  depends on  $l$  and the depth  $L$ . Therefore, in order to study the asymptotic information loss, we should specify how  $l$  grows relatively to  $L$ . In the next result, we study the two cases where  $l \ll L$  or  $l = \lfloor \alpha L \rfloor$ .

**Theorem 4** (Backward ILR). Let  $\epsilon \in (0, 1)$ , and define  $E_\epsilon = \{(x, x') \in (\sqrt{d}\mathbb{S}^d)^2 : \frac{1}{d}x \cdot x' < 1 - \epsilon\}$ . Under Assumptions 1 and 2, in the infinite width limit, we have the following results

- If  $l = \lfloor \alpha L \rfloor$  where  $\alpha \in (0, 1)$  is a constant, then there exists a constant  $\mu$  such that in the limit  $L \rightarrow \infty$ ,

$$\sup_{(x, x') \in E_\epsilon} |I_b^l(x, x') - \mu| = \Theta(\log(L)L^{-1})$$

- In the limit  $l, L \rightarrow \infty$  with  $l/L \rightarrow 0$ ,

$$\sup_{(x, x') \in E_\epsilon} |I_b^l(x, x')| = \Theta((L/l)^{-3})$$

---

3. In the sens that the layers adapt more effectively to data.

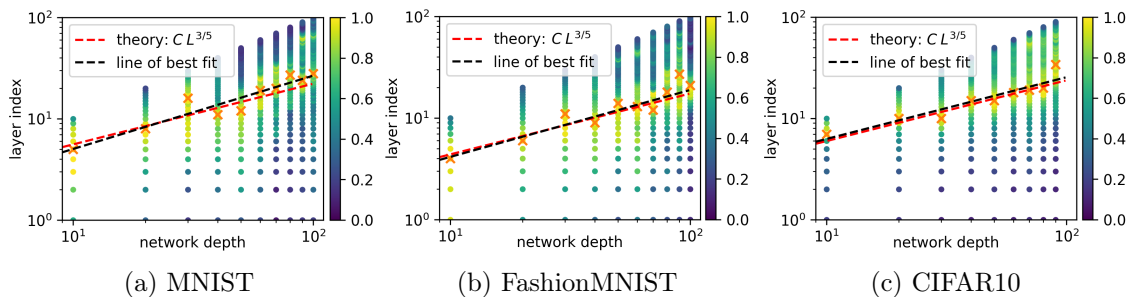


Figure 2: Data with  $x = 10j$  in the plot corresponds to layer alignments for a FFNN with depth  $10j$  trained on the MNIST/FashionMNIST/CIFAR10 datasets. The brighter the color, the closer the corresponding layer’s alignment is to the maximum alignment across all layers.  $\times$  indicates the layer where largest alignment occurs.

A key ingredient in the proof of Theorem 4 in the so-called Gradient Independence assumption. In the literature on signal propagation at initialization (e.g. (Schoenholz et al., 2017; Poole et al., 2016; Hayou et al., 2019; Yang and Schoenholz, 2017; Yang, 2019a; Xiao et al., 2018)), results on gradient backpropagation rely on the assumption that the weights used for backpropagation are independent from the ones used for forward propagation. Yang (2020) showed that this assumption yields exact computations of gradient covariance and NTK in the infinite width limit. We refer the reader to Appendix A.3 for more details.

In the case of infinite width FFNN, using Theorems 3 and 4, we derive a simple formula that characterizes the equilibrium.

**Corollary 5 (Equilibrium).** *Under the conditions of Theorems 3 and 4, the equilibrium for an FFNN is achieved for layers with index*

$$l = \Theta(L^{3/5})$$

where  $L$  is the network depth.

Corollary 5 indicates that the layers that satisfy the equilibrium property are those with indices  $l = \Theta(L^{3/5})$ . In logarithmic scale, this translates into a line  $\log(l) \in [\frac{3}{5} \log(L) + C_1, \frac{3}{5} \log(L) + C_2]$  where  $C_1, C_2$  are constants that depends on  $\epsilon$  from Theorems 3 and 4. Fig. 2 shows the layer CKAs after training an FFNN (width 256) on different datasets. We fit the line  $\log(l) = 3/5 \log(L) + C$  by finding the constant  $C$  that minimizes the squared error. We also perform a simple linear regression to see if the slope is close to  $3/5$  (line of best fit). All experiments show an excellent match with the theoretical line  $3/5 \log L + C$  (which was derived for infinite width networks).

**Gradient updates.** Let  $\mathbb{L}_m = \mathbb{L}(f(x_m), y_m)$  for  $m \in \{1, \dots, n\}$ . With an FFNN, the gradient of the loss w.r.t to some weight  $W_l^{ij}$  is given by

$$\frac{\partial \mathcal{L}}{\partial W_l^{ij}} = \frac{1}{n} \sum_{m=1}^n \frac{\partial \mathbb{L}_m}{\partial f(x_m)} \underbrace{\frac{\partial f_{l:L}(y_l^i(x_m))}{\partial y_l^i(x_m)}}_{\overleftarrow{\Psi}_{l,i}(x_m)} \underbrace{\phi(y_{l-1}^j(x_m))}_{\overrightarrow{\Psi}_{l,i}(x_m)}$$

where  $\vec{\Psi}_{l,i}$ , resp.  $\overleftarrow{\Psi}_{l,i}$ , is the feature map of forward, resp. backward, kernel. A key ingredient in the understanding of how the gradient behaves is the interaction between the terms  $(\vec{\Psi}_{l,i}(x_m))_{m \in [1:n]}$ ,  $(\overleftarrow{\Psi}_{l,i}(x_m))_{m \in [1:n]}$ . In the context of infinite width networks, neurons  $y_l^i$  are Gaussian processes, and thus are fully characterized by their covariance kernel. Hence, our intuition is to use the covariance between the forward/backward features as a measure of this interaction between the terms. When there is a balance between the forward/backward information flows, we would expect that both forward/backward features are expressive<sup>4</sup> and that the weight  $W_l^{ij}$  are more effectively trained. Leveraging this intuition, we use the second order geometry of neural networks in the next section to show how gradient updates is related to the evolution of layer CKA during early training steps, hence providing a clear idea of how EH impacts layer CKA during training.

#### 4. Alignment Hierarchy during training

The EH conjectures architectural advantage for some FFNN layers to more effectively learn features. Using second order geometry of DNNs, we depict the mechanisms by which the equilibrium property impacts how layer CKA evolves during early training. We restrict our analysis to the ReLU activation function, but the network could be of any type (FFNN, convolutional, etc.). We consider a classification task with  $k$  classes (i.e.  $o = k$ ). The loss function  $\mathbb{L}$  is the cross-entropy loss. We denote by  $F = (f_\theta(x_1)^T, f_\theta(x_2)^T, \dots, f_\theta(x_n)^T) \in \mathbb{R}^{nk}$  the concatenation of all outputs  $f_\theta(x_i)$  evaluated on the training dataset,  $w = \nabla_F \mathcal{L} \in \mathbb{R}^{nk}$  the gradient of the loss w.r.t to  $F$ ,  $Y \in \mathbb{R}^{nk}$  the concatenation of all one-hot vectors given by labels  $y_i$  in the dataset, and  $\tilde{Y} = \mathbf{C}Y$  the centered version of  $Y$ .

**Early training steps.** As shown in Fig. 1, layer CKAs sharply increase at early stages of training ( $\approx 2$  epochs of batch training), and plateau soon afterwards. We hence focus on the evolution of CKAs at early training (let  $T$  denote the total number of training epochs).

For ReLU activation (and more generally piecewise linear activations), we can express the gradient updates in terms of the output hessian matrix.

**Theorem 6.** *Gradient updates are given by*

$$\theta(t+1) = \left( \mathbf{I} - \frac{\eta}{L-1} \mathbf{H}_w(t) \right) \theta(t) \quad (8)$$

where, for  $v \in \mathbb{R}^{nk}$ ,  $\mathbf{H}_v = \sum_{x \in \mathcal{D}} \sum_{i=1}^k v_{x,i} \mathbf{H}^i(x)$ , and  $\mathbf{H}^i(x) = \frac{\partial^2 f_\theta^i(x)}{\partial \theta^2}$  is the output hessian evaluated at  $x$ . For  $v_{x,i}$ ,  $x$  indexes the datapoint and  $i$  the component.

Theorem 6 provides a geometric interpretation of gradient updates. The directions in parameter space where the largest updates occur are controlled by  $\mathbf{H}_w$ . A similar result holds for tangent features evolution during early training stages. Let us first introduce a key approximation.

**Approximation 1** (Collinearity at early training stages). *At early stages of training,  $\tilde{Y}$  and  $w$  are almost negatively co-linear. Specifically,  $w \approx -\frac{\|w\|}{\|\tilde{Y}\|} \tilde{Y}$ .*

---

4. Recall that the forward/backward signals degrade as the depth increases.

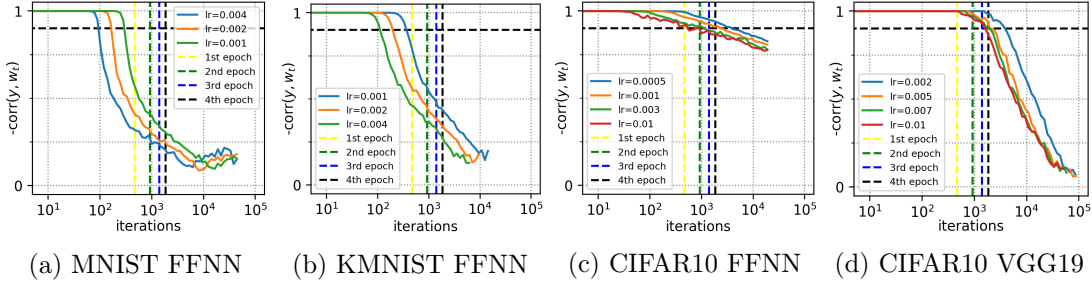


Figure 3: Empirical validation of Approximation 1: a demonstration that  $-\text{corr}(\tilde{Y}, w_t) \approx 1$  at early  $t$ .

The intuition behind Approximation 1 has roots in the assumption that the dataset is balanced. To see this, let  $(x, y) \in \mathcal{D}$  and  $\mathbb{L}_x = \mathbb{L}(f_\theta(x), y)$  the cross-entropy loss for the datapoint  $(x, y)$ . Let  $c$  be the true label of  $x$ , and  $i \in \{1, \dots, k\}$  such that  $i \neq c$ . We have that

$$\begin{aligned} \nabla_{f_\theta^i(x)} \mathcal{L} &= \frac{\exp(f_\theta^i(x))}{\sum_{j=1}^k \exp(f_\theta^j(x))}, \quad i \neq c \\ \nabla_{f_\theta^c(x)} \mathcal{L} &= - \sum_{i \neq c} \frac{\exp(f_\theta^i(x))}{\sum_{j=1}^k \exp(f_\theta^j(x))} \end{aligned} \quad (9)$$

where  $f_\theta^i(x)$  is the  $i$ -th entry of  $f_\theta(x)$ . When the dataset is balanced, i.e. the number of datapoint per class is approximately the same for all classes, the corresponding entries of  $\tilde{Y}$  satisfy  $\tilde{Y}_{x,c} \approx \frac{k-1}{k}$  and  $\tilde{Y}_{x,i} \approx \frac{-1}{k}$ . At initialization, with random weights,  $f_\theta^i(x)$  are on average similar across choices of  $x$  and  $i$ . Hence, using Eq. (9), on average we have  $w_{x,c} \approx -\frac{k-1}{k}$  and  $w_{x,i} \approx \frac{1}{k}$ , thus,  $\tilde{Y}$  are almost negatively co-linear. Fig. 3 illustrates this result on various architectures and datasets (see also Appendix D). We observe that Approximation 1 also holds during early training steps ( $\text{corr}(w, \tilde{Y}) \approx -1$  during the first training epoch). It turns out that Approximation 1 yields the following approximation for tangent features evolution during early training stages.

**Approximation 2** (Feature evolution). *The vectors  $\Psi(t+1)\tilde{Y} - \Psi(t)\tilde{Y}$  and  $-\eta \mathbf{H}_w(t)\Psi(t)\tilde{Y}$  are highly correlated.*

We refer the reader to Appendix B.5 for more theoretical insights on Approximation 2. Fig. 4a shows the correlation between the vectors  $U(\Psi(t+1)\tilde{Y} - \Psi(t)\tilde{Y})$  and  $-U\mathbf{H}_w(t)\Psi(t)\tilde{Y}$  during training for a depth 10 FFNN on CIFAR10, where  $U$  contains top 50 eigenvectors of  $U$  as its rows. As expected, they are highly correlated, especially during the early training stages.

From Theorem 6 and Approximation 2, the directions of the largest changes in parameters  $\theta$  are highly correlated with the directions of the largest changes in the vector  $\Psi\tilde{Y}$  which is the key component in the CKA. This provides a link that bridges the gap between the EH and effective feature learning. Indeed, from paragraph ‘‘Gradient updates’’ in Section 3, we explained our intuition on how the equilibrium property might be beneficial for parameter

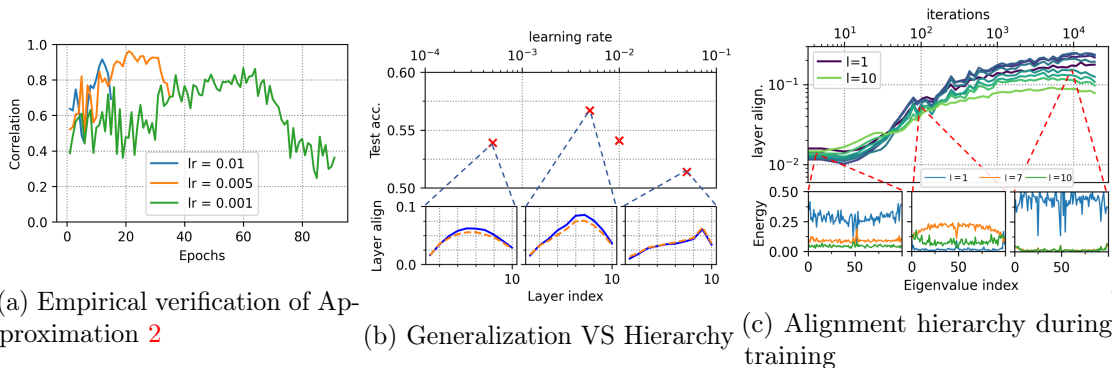


Figure 4: **(a)** Correlation between vectors  $U \left( \Psi(t+1)\tilde{Y} - \Psi(t)\tilde{Y} \right)$  and  $-U\mathbf{H}_w(t)\Psi(t)\tilde{Y}$  for CIFAR10 on a 10-layer FFNN. **(b)** Better layer alignment leads to better generalisation error, with a 10-layer FFNN on CIFAR10. Bottom panels show layer alignment for a selection of learning rates. **(c)** The norm of the eigenvectors of  $\mathbf{H}_w$  (energy in the plot) related to top 100 eigenvalues in absolute value projected to 3 layers: 1, 7, 10 at three training times. The top eigenvalues in absolute value of  $\mathbf{H}_w$  are 2, 15, 6 resp ( $\mathbf{H}_w$  has a symmetric eigenspectrum shown in Geiger et al. (2019)) for three training times. The plot provides an illustration of why alignment hierarchy arises as more energy of top eigenvectors concentrate on intermediate layers during critical increase in alignments.

updates in some layers that satisfy this property. On the other hand, Theorem 6 and Approximation 2 suggest that the directions with the largest updates in  $\theta$  are highly correlated with the directions for the largest updates in the vector  $\Psi\tilde{Y}$ . Hence, the equilibrium property might yield to effective updates in  $\Psi_l\tilde{Y}_l$  in the layers that satisfy this property.

To confirm this intuition, we train an depth 10 FFNN on CIFAR10 and show in Fig. 4c the norm of the top 100 eigenvectors of  $\mathbf{H}_w$  (corresponding to top 100 eigenvalues in absolute value) projected to 3 layers, extreme layer 1 and 10 and middle layer 7 (by projection to layer  $l$  we refer to the truncation of the vector to leave just the sub-vector that corresponds to layer  $l$ ). During the sharp increase phase in alignments (middle subfigure in Fig. 4c), the top eigenvectors of the Hessian are more concentrated on intermediate layers, suggesting that the sharpest increase in alignment occurs in those intermediate layers.

*Remark.* The hessian of the loss is given by  $\frac{\partial^2 \mathcal{L}}{\partial \theta^2} = \mathbf{H}_w + \Psi \frac{\partial^2 \mathcal{L}}{\partial F^2} \Psi^T := S + I$ . Previous works on second order geometry of DNNs (e.g. Karakida et al. (2019); Ghorbani et al. (2019)) focused on large positive eigenvalues of the loss hessian arising mostly from  $I$ . Approximation 2 shows that at the other end of the spectrum, large negative eigenvalues arising from  $S$  influences feature learning in 8. In particular, eigenvectors of  $S$  associated with large negative eigenvalues are directions of significant increase in alignment between features and labels.

## 5. Alignment and Generalization

To understand the impact of the alignment hierarchy on the generalization error, we train a depth 10 FFNN on CIFAR10 with a selection of learning rates and show the corresponding alignment hierarchy pattern for each one of them. Fig. 4b illustrates the results. It turns out that the best generalization error is the one with the sharpest increase in alignment. This

suggest that large alignments with data labels might indeed correlate with good generalization properties. For further experiments, including on random labels, see Appendix D.

## 6. Conclusion and Limitations

In this paper, we formulated and empirically validated the Equilibrium Hypothesis which links information flow at initialization to tangent features alignment with data labels, exhibiting an implicit layer selection regularization effect that arises solely from the *structure* of the network (deep networks). Our empirical results showed an excellent match with the theoretical prediction  $l = \Theta(L^{3/5})$  for FFNN on different datasets. Finally, using second order geometry, we show how EH is related to more effective evolution of tangent features in the layers that satisfy the equilibrium property. Extending the EH to other architecture is a promising topic for future research.

## References

- Aristide Baratin, Thomas George, César Laurent, R Devon Hjelm, Guillaume Lajoie, Pascal Vincent, and Simon Lacoste-Julien. Implicit regularization via neural feature alignment, 2021.
- Jeremy Bernstein and Yisong Yue. On the implicit biases of architecture & gradient descent. 2021.
- A. Camuto, M. Willetts, U. Simsekli, S. J. Roberts, and C. C. Holmes. Explicit regularisation in gaussian noise injections. In *Advances in Neural Information Processing Systems*, volume 33, pages 16603–16614, 2020.
- Jacopo Cavazza, Pietro Morerio, Benjamin Haeffele, Connor Lane, Vittorio Murino, and René Vidal. Dropout as a low-rank regularizer for matrix factorization. *arXiv preprint arXiv:1710.05092*, 2017.
- Mario Geiger, Stefano Spigler, Stephane d’Ascoli, Levent Sagun, Marco Baity-Jesi, Giulio Biroli, and Matthieu Wyart. Jamming transition as a paradigm to understand the loss landscape of deep neural networks. *Physical Review E*, 100(1):012115, 2019.
- Jonas Geiping, Micah Goldblum, Phillip E. Pope, Michael Moeller, and Tom Goldstein. Stochastic training is not necessary for generalization, 2021.
- Behrooz Ghorbani, Shankar Krishnan, and Ying Xiao. An investigation into neural net optimization via hessian eigenvalue density. In *International Conference on Machine Learning*, pages 2232–2241. PMLR, 2019.
- Priya Goyal, Piotr Dollár, Ross Girshick, Pieter Noordhuis, Lukasz Wesolowski, Aapo Kyrola, Andrew Tulloch, Yangqing Jia, and Kaiming He. Accurate, large minibatch sgd: Training imagenet in 1 hour. *arXiv preprint arXiv:1706.02677*, 2017.
- S. Hayou and F. Ayed. Regularization in resnet with stochastic depth. *Proceedings of Thirty-fifth Neural Information Processing Systems (NeurIPS)*, 2021.

- S. Hayou, A. Doucet, and J. Rousseau. On the impact of the activation function on deep neural networks training. In *International Conference on Machine Learning*, 2019.
- S. Hayou, A. Doucet, and J. Rousseau. Mean-field behaviour of neural tangent kernel for deep neural networks. *arXiv preprint arXiv:1905.13654*, 2020.
- K. He, X. Zhang, S. Ren, and J. Sun. Delving deep into rectifiers: Surpassing human-level performance on imagenet classification. *ICCV*, 2015.
- Geoffrey E Hinton, Nitish Srivastava, Alex Krizhevsky, Ilya Sutskever, and Ruslan R Salakhutdinov. Improving neural networks by preventing co-adaptation of feature detectors. *arXiv preprint arXiv:1207.0580*, 2012.
- Gao Huang, Yu Sun, Zhuang Liu, Daniel Sedra, and Kilian Q Weinberger. Deep networks with stochastic depth. In *European conference on computer vision*, pages 646–661. Springer, 2016.
- A. Jacot, F. Gabriel, and C. Hongler. Neural tangent kernel: Convergence and generalization in neural networks. In *Advances in Neural Information Processing Systems*, 2018.
- Arthur Jacot, Franck Gabriel, and Clément Hongler. The asymptotic spectrum of the hessian of dnn throughout training, 2020.
- Stanislaw Jastrzebski, Zachary Kenton, Devansh Arpit, Nicolas Ballas, Asja Fischer, Yoshua Bengio, and Amos J Storkey. Finding flatter minima with sgd. In *ICLR (Workshop)*, 2018.
- Ryo Karakida, Shotaro Akaho, and Shun-ichi Amari. Universal statistics of fisher information in deep neural networks: Mean field approach. In *The 22nd International Conference on Artificial Intelligence and Statistics*, pages 1032–1041. PMLR, 2019.
- Alex Krizhevsky, Ilya Sutskever, and Geoffrey E Hinton. Imagenet classification with deep convolutional neural networks. 2012.
- Mandar Kulkarni and Shirish Karande. Layer-wise training of deep networks using kernel similarity. *arXiv preprint arXiv:1703.07115*, 2017.
- Y. Lecun, L. Bottou, Y. Bengio, and P. Haffner. Gradient-based learning applied to document recognition. *Proceedings of the IEEE*, 86(11):2278–2324, 1998. doi: 10.1109/5.726791.
- J. Lee, Y. Bahri, R. Novak, S.S. Schoenholz, J. Pennington, and J. Sohl-Dickstein. Deep neural networks as Gaussian processes. In *International Conference on Learning Representations*, 2018.
- J. Lee, L. Xiao, S. Schoenholz, Y. Bahri, J. Sohl-Dickstein, and J. Pennington. Wide neural networks of any depth evolve as linear models under gradient descent. *NeurIPS*, 2019a.
- Jaehoon Lee, Lechao Xiao, Samuel Schoenholz, Yasaman Bahri, Roman Novak, Jascha Sohl-Dickstein, and Jeffrey Pennington. Wide neural networks of any depth evolve as linear models under gradient descent. *Advances in neural information processing systems*, 32:8572–8583, 2019b.

- Jaehoon Lee, Samuel S Schoenholz, Jeffrey Pennington, Ben Adlam, Lechao Xiao, Roman Novak, and Jascha Sohl-Dickstein. Finite versus infinite neural networks: an empirical study. *arXiv preprint arXiv:2007.15801*, 2020.
- T. Lillicrap, D. Cownden, D. Tweed, and C. Akerman. Random synaptic feedback weights support error backpropagation for deep learning. *Nature Communications*, 7(13276), 2016.
- A.G. Matthews, J. Hron, M. Rowland, R.E. Turner, and Z. Ghahramani. Gaussian process behaviour in wide deep neural networks. In *International Conference on Learning Representations*, 2018.
- Alexander G de G Matthews, Jiri Hron, Richard E Turner, and Zoubin Ghahramani. Sample-then-optimize posterior sampling for bayesian linear models. In *NeurIPS Workshop on Advances in Approximate Bayesian Inference*, 2017.
- Poorya Mianjy and Raman Arora. On dropout and nuclear norm regularization. *arXiv preprint arXiv:1905.11887*, 2019.
- Chris Mingard, Guillermo Valle-Pérez, Joar Skalse, and Ard A Louis. Is sgd a bayesian sampler? well, almost. *Journal of Machine Learning Research*, 22(79):1–64, 2021.
- R.M. Neal. *Bayesian Learning for Neural Networks*, volume 118. Springer Science & Business Media, 1995.
- B. Poole, S. Lahiri, M. Raghu, J. Sohl-Dickstein, and S. Ganguli. Exponential expressivity in deep neural networks through transient chaos. *30th Conference on Neural Information Processing Systems*, 2016.
- S.S. Schoenholz, J. Gilmer, S. Ganguli, and J. Sohl-Dickstein. Deep information propagation. In *International Conference on Learning Representations*, 2017.
- Haozhe Shan and Blake Bordelon. Rapid feature evolution accelerates learning in neural networks, 2021.
- Guillermo Valle-Perez, Chico Q Camargo, and Ard A Louis. Deep learning generalizes because the parameter-function map is biased towards simple functions. *arXiv preprint arXiv:1805.08522*, 2018.
- Stefan Wager, Sida Wang, and Percy S Liang. Dropout training as adaptive regularization. In *Advances in neural information processing systems*, pages 351–359, 2013.
- C. Wei, S. Kakade, and T. Ma. The implicit and explicit regularization effects of dropout. In *Proceedings of the 37th International Conference on Machine Learning*, Proceedings of Machine Learning Research, pages 10181–10192. PMLR, 2020.
- Jingfeng Wu, Wenqing Hu, Haoyi Xiong, Jun Huan, Vladimir Braverman, and Zhanxing Zhu. On the noisy gradient descent that generalizes as sgd. In *International Conference on Machine Learning*, pages 10367–10376. PMLR, 2020.
- Lei Wu, Zhanxing Zhu, et al. Towards understanding generalization of deep learning: Perspective of loss landscapes. *arXiv preprint arXiv:1706.10239*, 2017.

- L. Xiao, Y. Bahri, J. Sohl-Dickstein, S. S. Schoenholz, and P. Pennington. Dynamical isometry and a mean field theory of cnns: How to train 10,000-layer vanilla convolutional neural networks. *ICML 2018*, 2018.
- G. Yang. Scaling limits of wide neural networks with weight sharing: Gaussian process behavior, gradient independence, and neural tangent kernel derivation. *arXiv preprint arXiv:1902.04760*, 2019a.
- G. Yang. Tensor programs i: Wide feedforward or recurrent neural networks of any architecture are Gaussian processes. *arXiv preprint arXiv:1910.12478*, 2019b.
- G. Yang. Tensor programs iii: Neural matrix laws. *arXiv preprint arXiv:2009.10685*, 2020.
- G. Yang and S. Schoenholz. Mean field residual networks: On the edge of chaos. In *Advances in neural information processing systems*, pages 7103–7114, 2017.
- Chiyuan Zhang, Samy Bengio, Moritz Hardt, Benjamin Recht, and Oriol Vinyals. Understanding deep learning (still) requires rethinking generalization. *Communications of the ACM*, 64(3):107–115, 2021.

## Appendix A. Review of Signal propagation theory

The signal propagation theory in the context of neural networks deals precisely with the distortion of the information carried by the output as it travels through the network. Most results in this theory (see e.g. [Poole et al. \(2016\)](#); [Schoenholz et al. \(2017\)](#); [Yang \(2020\)](#); [Hayou et al. \(2020, 2019\)](#); [Jacot et al. \(2018, 2020\)](#)) consider the infinite width limit as it allows the derivation of closed-form expressions. Infinite width networks are also naturally overparameterized (infinite number of parameters) and therefore might offer some theoretical insights on the overparameterized regime.

**Fully-connected FeedForward Neural Networks (FFNN).** Given an input  $x \in \mathbb{R}^d$ , and a set of weights and bias  $(W_l, b_l)_{1 \leq l \leq L}$ , the forward propagation is given by

$$z_1(x) = W_1 x + b_1 \tag{1}$$

$$z_l(x) = W_l \phi(z_{l-1}(x)), \quad 2 \leq l \leq L, \tag{2}$$

where  $W_l \in \mathbb{R}^{N_l \times N_{l-1}}$ , and  $\phi$  is the ReLU activation function given by  $\phi(v) = \max(v, 0)$  for  $v \in \mathbb{R}$ . The dimension of the parameter space is  $P = \sum_{l=0}^{L-1} (N_l + 1) N_{l+1}$  where we denote  $N_0 := d$ . For each layer, the weights are initialized with i.i.d Gaussian variables  $W_l^{ij} \sim \mathcal{N}(0, \frac{2}{N_{l-1}})$ .

### A.1 Forward propagation

When we take the limit  $N_{l-1} \rightarrow \infty$  recursively over  $l$ , this implies, using Central Limit Theorem, that  $z_l^i(x)$  is a Gaussian random variable for any input  $x$ . The convergence rate to this limiting Gaussian distribution is given  $\mathcal{O}(1/\sqrt{N_{l-1}})$  (standard Monte Carlo error). More generally, an approximation of the random process  $z_l^i(\cdot)$  by a Gaussian process was first proposed by [Neal \(1995\)](#) in the single layer case and has been extended to the multiple layer case by [Lee et al. \(2018\)](#) and [Matthews et al. \(2018\)](#). The limiting Gaussian process kernels follow a recursive formula given by, for any inputs  $x, x' \in \mathbb{R}^d$

$$\begin{aligned} \kappa_l(x, x') &= \mathbb{E}[z_l^i(x) z_l^i(x')] \\ &= 2 \mathbb{E}[\phi(z_{l-1}^i(x)) \phi(z_{l-1}^i(x'))] \\ &= 2 \Psi_\phi(\kappa_{l-1}(x, x), \kappa_{l-1}(x, x'), \kappa_{l-1}(x', x')), \end{aligned}$$

where  $\Psi_\phi$  is a function that only depends on  $\phi$ . This provides a simple recursive formula for the computation of the kernel  $\kappa^l$ ; see, e.g., [Lee et al. \(2018\)](#) for more details.

### A.2 Gradient Independence

In the literature of infinite width DNNs, a standard assumption in prior literature is that of the gradient independence which is similar in nature to the concept of feedback alignment ([Lillicrap et al., 2016](#)). This assumption states that, for infinitely wide neural networks, if we assume the weights used for forward propagation are independent from those used for back-propagation. When used for the computation of Neural Tangent Kernel, this approximation was proven to give the exact computation for standard architectures such as FFNN, CNN and ResNets [Yang \(2020\)](#).

**Lemma 1** (Corollary of Theorem D.1. in (Yang, 2020)). *Consider an FFNN with weights  $\mathbf{W}$ . In the limit of infinite width, we can assume that  $\mathbf{W}^T$  used in back-propagation is independent from  $\mathbf{W}$  used for forward propagation, for the calculation of Gradient Covariance and NTK.*

This result has been extensively used in the literature as an approximation before being proved to yield exact computation for gradient covariance and NTK.

**Gradient Covariance back-propagation.** Analytical formulas for gradient covariance back-propagation were derived using this result, in (Hayou et al., 2019; Schoenholz et al., 2017; Poole et al., 2016; Xiao et al., 2018; Yang, 2019a). Empirical results showed an excellent match for FFNN in Schoenholz et al. (2017), for Resnets in Yang (2019a) and for CNN in Xiao et al. (2018).

**Neural Tangent Kernel.** The Gradient Independence approximation was implicitly used in Jacot et al. (2018) to derive the infinite width Neural Tangent Kernel (See Jacot et al. (2018), Appendix A.1). The authors have found that the infinite width NTK computed with the Gradient Independence approximation yields excellent match with empirical (exact) NTK.

### A.3 Back-propagation

For FFNN layers, let  $q_l(x) := q_l(x, x)$  be the variance of  $z_l^1(x)$  (the choice of the index 1 is not important since, in the infinite width limit, the random variables  $(z_l^i(x))_{i \in [1:N_l]}$  are i.i.d). Let  $q_l(x, x')$ , resp.  $c_l^1(x, x')$  be the covariance, resp. the correlation between  $z_l^1(x)$  and  $z_l^1(x')$ . For Gradient back-propagation, let  $\tilde{q}_l(x, x')$  be the Gradient covariance defined by  $\tilde{q}_l(x, x') = \mathbb{E} \left[ \frac{\partial \mathcal{L}}{\partial z_l^1}(x) \frac{\partial \mathcal{L}}{\partial z_l^1}(x') \right]$  where  $\mathcal{L}$  is some loss function. Similarly, let  $\tilde{q}_l(x)$  be the Gradient variance at point  $x$ . We also define  $\hat{q}_l(x, x') = 2\mathbb{E}[\phi'(z_{l-1}^1(x))\phi'(y_{l-1}^1(x'))]$ .

Given two inputs  $x, x' \in \mathbb{R}^d$ , using Central Limit Theorem as in Schoenholz et al. (2017), we obtain

$$q_l(x, x') = 2\mathbb{E} \left[ \phi \left( \sqrt{q_l(x)} Z_1 \right) \phi \left( \sqrt{q_l(x')} (c^{l-1} Z_1 + \sqrt{1 - (c^{l-1})^2} Z_2) \right) \right], \quad Z_1, Z_2 \stackrel{iid}{\sim} \mathcal{N}(0, 1),$$

with  $c^{l-1} := c^{l-1}(x, x')$ .

With ReLU, and since ReLU is positively homogeneous (i.e.  $\phi(\lambda x) = \lambda \phi(x)$  for  $\lambda \geq 0$ ), we have that

$$q_l(x, x') = \sqrt{q^l(x)} \sqrt{q^l(x')} g(c^{l-1})$$

where  $g$  is the ReLU correlation function given by ?

$$g(c) = \frac{1}{\pi} (c \arcsin c + \sqrt{1 - c^2}) + \frac{1}{2} c. \quad (3)$$

**Gradient back-propagation.** The gradient back-propagation is given by

$$\frac{\partial f_{l:L}}{\partial y_i^l} = \phi'(y_i^l) \sum_{j=1}^{N_{l+1}} \frac{\partial f_{l:L}}{\partial y_j^{l+1}} W_{ji}^{l+1}.$$

where  $f_{l:L}$  is the mapping from layer  $l$  to the output. Using the Gradient Independence in the infinite width limit (Lemma 1) and under Assumption 2, a Central Limit Theorem argument yields (see e.g. Section 7.9 in the appendix in Schoenholz et al. (2017))

$$\tilde{q}_l(x, x') = \tilde{q}_{l+1}(x, x')g'(c_l(x, x')),$$

where  $g$  is the function defined in Eq. (3).

By telescopic product, we obtain

$$\tilde{q}_l(x, x') = \tilde{q}_L(x, x') \prod_{k=l}^{L-1} g'(c_k(x, x')) = \tilde{q}_L(x, x') \frac{\zeta_L(x, x')}{\zeta_l(x, x')}. \quad (4)$$

where  $\zeta_m(x, x') = \prod_{k=1}^{m-1} g'(c_k(x, x'))$  for  $m \geq 2$ .

#### A.4 Standard parameterization Vs NTK parameterization

Many papers that study the NTK consider the so-called NTK parameterization given by

$$z_1(x) = \frac{2}{\sqrt{d}} W_1 x + b_1 \quad (5)$$

$$z_l(x) = \frac{2}{\sqrt{N_{l-1}}} W_l \phi(z_{l-1}(x)), \quad 2 \leq l \leq L, \quad (6)$$

where the weights  $W_l^{ij}$  are initialized with standard normal distribution  $\mathcal{N}(0, 1)$ . However, both parameterizations yield the same quantities for signal propagation at initialization, i.e. the covariance  $q_l$  is the same for both parameterizations. In our proofs, we will refer to results in Hayou et al. (2020) and Schoenholz et al. (2017) that consider either the NTK or the standard parameterization.

## Appendix B. Proofs

### B.1 Proof of Theorem 3

**Theorem 3** (Forward Information Loss). *Let  $\epsilon \in (0, 1)$ , and define  $E_\epsilon = \{(x, x') \in (\sqrt{d}\mathbb{S}^d)^2 : \frac{1}{d}x \cdot x' < 1 - \epsilon\}$ . Under Assumption 1, the sequence  $(I_f^l)_{l \geq 1}$  has an information loss rate of  $r_l = l^{-2}$  over  $E$ . More precisely,*

$$\sup_{(x, x') \in E_\epsilon} |I_f^l(x, x') - 1/2| = \Theta(l^{-2})$$

Theorem 3 is a corollary of a previous result that appeared in Hayou et al. (2020). The proof techniques for the latter rely on an asymptotic analysis of a well defined covariance kernel in the limit of large  $l$ , coupled with a uniform bounding of the convergence rate.

*Proof.* Fix  $(x, x') \in E$ . Define the covariance between  $z_l^1(x), z_l^1(x')$  by

$$q_l(x, x') = \mathbb{E}[z_l^1(x)z_l^1(x)']$$

In the infinite width limit, it is straightforward

Since  $q_1(x, x) = q_1(x', x') = 1$ ,  $q_1(x, x')$  can be seen as the correlation between  $z_1^1(x)$  and  $z_1^1(x')$ . Recursively, it is straightforward that  $q_l(x, x) = q_l(x', x') = 1$  for all  $l$ , suggesting that  $q_l(x, x')$  can be seen as the correlation between  $z_l^1(x)$  and  $z_l^1(x')$ . We also observe that  $q_l(x, x') = 2I_f^l(x, x')$ .

From Appendix Lemma 1 in [Hayou et al. \(2020\)](#), we have that

$$\sup_{(x, x') \in E_\epsilon} |q_l(x, x') - 1| = \Theta(l^{-2})$$

which yields the desired result.  $\square$

## B.2 Proof of Theorem 4

We first prove a result that will be useful in the proof of Theorem 4.

**Lemma 2** (Uniform Asymptotic Expansion). *Let  $a \geq 1$  be a positive integer. We define the sequence  $(b_l)_{l \geq 0}$  by*

$$b_l = \beta_l b_{l-1},$$

where  $(\beta_l)_{l \geq 0}$  is a sequence of reals numbers that satisfy  $\beta_l = 1 - \frac{a}{l} + \kappa \frac{\log(l)}{l^2} + \mathcal{O}(l^{-2})$  where  $\kappa \neq 0$  is a constant that does not depend on  $\beta_0$ . Assume that the  $\mathcal{O}$  bound is uniform over  $\beta_0$ . Then, uniformly over  $\beta_0$ , we have that

$$\log(b_l) = -a \log(l) + \kappa \frac{\log(l)}{l} + \mathcal{O}(l^{-1})$$

*Proof.* Let  $r_l := b_l l^a$ . We have that

$$\begin{aligned} r_l &= b_l r_{l-1} (1 + a l^{-1} + \mathcal{O}(l^{-2})) \\ &= (1 + \kappa \frac{\log(l)}{l^2} + \mathcal{O}(l^{-2})) r_{l-1} \end{aligned}$$

which yields

$$\log(r_l/r_{l-1}) = \kappa \frac{\log(l)}{l^2} + \mathcal{O}(l^{-2})$$

Since the series on the right side converge, we have that

$$\begin{aligned} \sum_{k \geq l} \log(r_k/r_{k-1}) &= \sum_{k \geq l} \kappa \frac{\log(k)}{k^2} + \mathcal{O}(\sum_{k \geq l} k^{-2}) \\ &= -\kappa \frac{\log(l) + 1}{l} + \mathcal{O}(\log(l)l^{-2}) + \mathcal{O}(l^{-1}) \\ &= -\kappa \frac{\log(l)}{l} + \mathcal{O}(l^{-1}) \end{aligned}$$

$\square$

where we have use the integral estimates of the remainders of series. Since the  $\mathcal{O}$  bound in  $\beta_l$  is uniform over  $\beta_0$  by assumption, then the resulting  $\mathcal{O}$  bound in  $\log(r_l)$  is also uniform over  $\beta_0$ , which concludes the proof.

**Theorem 4** (Backward Information Loss). *Let  $\epsilon \in (0, 1)$ , and define  $E_\epsilon = \{(x, x') \in (\sqrt{d}\mathbb{S}^d)^2 : \frac{1}{d}x \cdot x' < 1 - \epsilon\}$ . Under Assumptions 1 and 2, in the infinite width limit, we have the following results:*

- If  $l = \lfloor \alpha L \rfloor$  where  $\alpha \in (0, 1)$  is a constant, then there exists a constant  $\kappa$  such that in the limit  $L \rightarrow \infty$ ,

$$\sup_{(x, x') \in E_\epsilon} |I_b^l(x, x') - \kappa| = \Theta(\log(L)L^{-1})$$

- In the limit  $l, L \rightarrow \infty$  with  $l/L \rightarrow 0$ ,

$$\sup_{(x, x') \in E_\epsilon} |I_b^l(x, x')| = \Theta((L/l)^{-3})$$

*Proof.* Let  $\epsilon \in (0, 1)$ . Note that  $I_b^l(x, x') = \tilde{q}_l(x, x')$  where  $\tilde{q}_l$  is defined in Appendix A.3.

Using a Taylor expansion of  $g$  near 1, Appendix Lemma 1 in Hayou et al. (2020) shows that there exists a constant  $\kappa > 0$  such that

$$\sup_{(x, x') \in E} |g'(c_l(x, x')) - 1 + \frac{3}{l} - \kappa \frac{\log(l)}{l^2}| = \mathcal{O}(l^{-2})$$

Let  $\zeta_l(x, x') = \prod_{k=1}^{l-1} g'(c_k(x, x'))$  as in Appendix A.3. It is clear that  $(\zeta_l)$  satisfies the conditions in Lemma 2. Hence, letting  $r_l = \zeta_l(x, x') l^3$ <sup>5</sup>, we obtain

$$\log(r_l) = \kappa \frac{\log(l)}{l} + \mathcal{O}(l^{-1})$$

where the  $\mathcal{O}$  bound is uniform over  $(x, x') \in E$ .

The loss function is given by  $\mathbb{L}(f(x), y)$ , therefore  $\tilde{q}_L(x, x') = \mathbb{E}[\frac{\partial \mathbb{L}(f(x), y)}{\partial z_L^1(x)} \frac{\partial \mathbb{L}(f(x'), y')}{\partial z_L^1(x')}]$ . Using the result on the correlation propagation from Appendix Lemma 1 in Hayou et al. (2020), we obtain that  $\tilde{q}_L(x, x') = \tilde{q} + \mathcal{O}(L^{-2})$  as  $L$  goes to infinity, where  $\tilde{q}$  is independent of  $(x, x')$ .

Now let us discuss the two cases:

- Case 1 ( $l = \lfloor \alpha L \rfloor$ ): in this case, we have that  $\log(r_L) - \log(r_{\lfloor \alpha L \rfloor}) = \Theta(\log(L)L^{-1})$ , which yields

$$\frac{\zeta_L(x, x')}{\zeta_{\lfloor \alpha L \rfloor}(x, x')} = \alpha^3 + \Theta(\log(L)L^{-1})$$

where  $\Theta$  is uniform over  $x, x'$ . This proves that

$$\sup_{(x, x') \in E} |\tilde{q}_{\lfloor \alpha L \rfloor}(x, x') - \alpha^3 \tilde{q}| = \Theta(\log(L)L^{-1})$$

- Case 2 ( $l/L \rightarrow 0$ ): in this case, we have that

$$\frac{\zeta_L(x, x')}{\zeta_l(x, x')} \sim (L/l)^{-3},$$

---

5. We omit  $(x, x')$  to alleviate the notations.

uniformly over  $x, x'$ . We conclude that

$$\sup_{(x, x') \in E} |\tilde{q}_l(x, x')| = \Theta((L/l)^{-3}).$$

□

### B.3 Proof of Corollary 5

**Corollary 5** (Equilibrium). *Under the conditions of Theorems 3 and 4, the equilibrium for an FFNN is achieved for layers with index*

$$l = \Theta(L^{3/5})$$

where  $L$  is the network depth.

*Proof.* We have two cases:

- If  $l$  is of the same order as  $L$ , or simply  $l = \lfloor \alpha L \rfloor$  where  $\alpha \in (0, 1)$  is a constant, then to have the equilibrium property, we need to have  $l^{-2} = \Theta(\log(L)L^{-1})$  which is absurd. Hence, equilibrium cannot be achieved in this case.
- Therefore, the only possible scenario where equilibrium can be achieved is when  $l/L \rightarrow 0$ , in this case, the equilibrium property implies  $l^{-2} = \Theta((L/l)^{-3})$  which yields

$$l = \Theta(L^{3/5})$$

□

### B.4 Proof of Theorem 6

*Proof.* Let  $\mathbf{B}_{l_1, l_2}$  be the block in  $\mathbf{H}^i(x)$  containing all entries of the form  $\frac{\partial^2 f^i(x)}{\partial W_{l_1}^{jk} \partial W_{l_2}^{st}}$  where  $W_{l_1}^{jk}$  is one of layer  $l_1$ 's parameters, and  $W_{l_2}^{st}$  one of layer  $l_2$ 's parameters.

If  $l_1 = l_2$ , by piecewise linearity of  $\phi$ ,  $\mathbf{B}_{l_1, l_2}$  contains all zero entries.

If  $l_1 > l_2$ , fixing  $W_{l_1}^{jk}$ ,

$$\frac{\partial^2 f^i(x)}{\partial W_{l_1}^{jk} \partial W_{l_2}^{st}} = \frac{\partial \phi(z_{l_1-1}^k(x))}{\partial W_{l_2}^{st}} \frac{\partial f^i(x)}{\partial z_{l_1}} [j]$$

where  $\frac{\partial f^i(x)}{\partial z_{l_1}} [j]$  is the  $j$ -th entry of  $\frac{\partial f^i(x)}{\partial z_{l_1}}$ . Hence

$$\sum_{s,t} \frac{\partial^2 f^i(x)}{\partial W_{l_1}^{jk} \partial W_{l_2}^{st}} W_{l_2}^{st} = \left( \sum_{s,t} \frac{\partial \phi(z_{l_1-1}^k(x))}{\partial W_{l_2}^{st}} W_{l_2}^{st} \right) \frac{\partial f^i(x)}{\partial z_{l_1}} [j]$$

By piecewise linearity of activation function,

$$\sum_{s,t} \frac{\partial^2 f^i(x)}{\partial W_{l_1}^{jk} \partial W_{l_2}^{st}} W_{l_2}^{st} = \phi(z_{l_1-1}^k(x)) \frac{\partial f^i(x)}{\partial z_{l_1}} [j] = \frac{\partial f^i(x)}{\partial W_{l_1}^{jk}}$$

If  $l_1 < l_2$ , fixing  $W_{l_1}^{jk}$ ,

$$\frac{\partial^2 f^i(x)}{\partial W_{l_1}^{jk} \partial W_{l_2}^{st}} = \phi(z_{l_1-1}^k(x)) \frac{\partial \frac{\partial f^i(x)}{\partial z_{l_1}}[j]}{\partial W_{l_2}^{st}}$$

Using piecewise linearity of activation function again, we get:

$$\sum_{s,t} \frac{\partial^2 f^i(x)}{\partial W_{l_1}^{jk} \partial W_{l_2}^{st}} W_{l_2}^{st} = \phi(z_{l_1-1}^k(x)) \left( \sum_{s,t} \frac{\partial \frac{\partial f^i(x)}{\partial z_{l_1}}[j]}{\partial W_{l_2}^{st}} W_{l_2}^{st} \right) = \phi(z_{l_1-1}^k(x)) \frac{\partial f^i(x)}{\partial z_{l_1}}[j] = \frac{\partial f^i(x)}{\partial W_{l_1}^{jk}}$$

Combining the above results we get: (fixing  $l_1 \in \{1, \dots, L\}$ , for any  $W_{l_1}^{jk}$ )

$$\sum_{l_2=1}^L \sum_{s,t} \frac{\partial^2 f^i(x)}{\partial W_{l_1}^{jk} \partial W_{l_2}^{st}} W_{l_2}^{st} = (L-1) \frac{\partial f^i(x)}{\partial W_{l_1}^{jk}}$$

The left hand side is the entry of  $\mathbf{H}^i(x)\theta$  corresponding to parameter  $W_{l_1}^{jk}$ , the right hand side is the entry of  $(L-1)\Psi^i(x)$  corresponding to parameter  $W_{l_1}^{jk}$ . Therefore we yield:

$$\Psi^i(x) = \frac{1}{L-1} \mathbf{H}^i(x)\theta$$

By this result, the gradient of loss w.r.t parameters can be written as:

$$\nabla_{\theta} \mathcal{L} = \left( \frac{\partial \mathcal{L}}{\partial F} \frac{\partial F}{\partial \theta} \right)^T = (w^T \Psi^T)^T = \Psi w = \frac{\eta}{L-1} \mathbf{H}_w(t)\theta(t)$$

Hence, gradient updates are given by

$$\theta(t+1) = \left( \mathbf{I} - \frac{\eta}{L-1} \mathbf{H}_w(t) \right) \theta(t)$$

□

## B.5 Justification of Approximation 2

**Approximation 3** (1<sup>st</sup> order approximation).

$$\Psi^i(x)(t+1) - \Psi^i(x)(t) = \mathbf{H}^i(x)(t) (\theta(t+1) - \theta(t)) + \mathcal{E}_{x,i}(t)$$

where  $\mathcal{E}_{x,i}(t)$  includes higher order terms of  $\theta(t+1) - \theta(t)$ . We will first justify Approximation 3:

$$\begin{aligned} \Psi^i(x)(t+1) - \Psi^i(x)(t) &= \left. \frac{\partial f^i(x)}{\partial \theta} \right|_{\theta(t+1)} - \left. \frac{\partial f^i(x)}{\partial \theta} \right|_{\theta(t)} \\ &= \left. \frac{\partial^2 f^i(x)}{\partial \theta^2} \right|_{\theta(t)} (\theta(t+1) - \theta(t)) + \mathcal{E}_{x,i}(t) \\ &= \mathbf{H}^i(x)(t) (\theta(t+1) - \theta(t)) + \mathcal{E}_{x,i}(t) \end{aligned}$$

The second step is by Taylor expanding  $\left. \frac{\partial f^i(x)}{\partial \theta} \right|_{\theta(t+1)}$  around  $\theta(t)$ . Given Approximation 3, for an arbitrary fixed vector  $v \in \mathbb{R}^{kn}$ , the evolution of  $\Psi v$  can be approximated by:

$$\begin{aligned}
\Psi(t+1)v - \Psi(t)v &= \sum_{x \in \mathcal{D}} \sum_{j=1}^k v_{x,i} (\mathbf{H}^i(x)(t) (\theta(t+1) - \theta(t)) + \mathcal{E}_{x,i}(t)) \\
&= -\eta \sum_{x \in \mathcal{D}} \sum_{j=1}^k v_{x,i} \mathbf{H}^i(x)(t) \Psi(t)w + \sum_{x \in \mathcal{D}} \sum_{j=1}^k v_{x,i} \mathcal{E}_{x,i}(t) \quad (7) \\
&= -\eta \mathbf{H}_v(t) \Psi(t)w + \sum_{x \in \mathcal{D}} \sum_{j=1}^k v_{x,i} \mathcal{E}_{x,i}(t)
\end{aligned}$$

Setting  $v = \tilde{Y}$  we get:

$$\begin{aligned}
\Psi(t+1)\tilde{Y} &= \Psi(t)\tilde{Y} - \eta \mathbf{H}_{\tilde{Y}} \Psi(t)w + \sum_{x \in \mathcal{D}} \sum_{j=1}^k \tilde{Y}_{x,i} \mathcal{E}_{x,i}(t) \\
&\approx \Psi(t)\tilde{Y} - \eta \mathbf{H}_w \Psi(t)\tilde{Y} + \sum_{x \in \mathcal{D}} \sum_{j=1}^k \tilde{Y}_{x,i} \mathcal{E}_{x,i}(t) \quad (8) \\
&= (\mathbf{I} - \eta \mathbf{H}_w) \Psi(t)\tilde{Y} + \sum_{x \in \mathcal{D}} \sum_{j=1}^k \tilde{Y}_{x,i} \mathcal{E}_{x,i}(t)
\end{aligned}$$

In the second step we use Approximation 1. As  $\sum_{x \in \mathcal{D}} \sum_{j=1}^k \tilde{Y}_{x,i} \mathcal{E}_{x,i}(t)$  contains high order terms in  $\eta$ , this is small compared to  $(\mathbf{I} - \eta \mathbf{H}_w) \Psi(t)\tilde{Y}$ . Hence, the update in feature vector  $\Psi(t+1)\tilde{Y} - \Psi(t)\tilde{Y}$  is highly correlated with  $-\eta \mathbf{H}_w \Psi(t)\tilde{Y}$ .

## Appendix C. Optimal Feature Evolution Scheme

Shan and Bordelon (2021) proposed Optimal Feature Evolution (OFE) scheme to model the evolution of tangent features during gradient descent (GD) training. Under OFE, the tangent features  $\Psi$  evolve greedily so that the change in empirical loss  $\mathcal{L}$  is maximised at each time step. However, it is not verified empirically if OFE matches any variants of GD methods. In the following, we propose Generalised Optimal Feature Evolution (GOFE) scheme to capture GD methods more closely and gain insights into the evolution of layerwise CKA.

### C.1 Optimal Feature Evolution with fixed learning rates

In Shan and Bordelon (2021), the optimal feature evolution paradigm is only given for MSE loss. The following is a summary of OFE evolution scheme for any twice differentiable loss  $\mathcal{L}$ . We inherit notation from Section 4.

By GD training dynamics we have:

$$\begin{aligned}
\frac{\partial \theta^T}{\partial t} &= -\eta \frac{\partial \mathcal{L}}{\partial \theta} = -\eta \frac{\partial \mathcal{L}}{\partial F} \frac{\partial F}{\partial \theta} \\
&= -\eta w^T \Psi^T \\
\Rightarrow \frac{\partial \theta}{\partial t} &= -\eta \Psi w
\end{aligned} \tag{9}$$

The evolution of  $\mathcal{L}$  is:

$$\frac{\partial \mathcal{L}}{\partial t} = \frac{\partial \mathcal{L}}{\partial F} \frac{\partial F}{\partial \theta} \frac{\partial \theta}{\partial t} = -\eta w^T \Psi^T \Psi w \tag{10}$$

Using the same argument as in [Shan and Bordelon \(2021\)](#), we optimise the term  $w^T \Psi^T \Psi w$  w.r.t  $\Psi$  by evolving  $\Psi$  in the direction of largest decrease in  $-w^T \Psi^T \Psi w$  with a learning rate of  $\lambda$ . This yield:

$$\begin{aligned}
\frac{\partial \Psi^T}{\partial t} &= -\lambda \frac{\partial (-\eta w^T \Psi^T \Psi w)}{\partial \Psi} \\
\Rightarrow \frac{\partial \Psi}{\partial t} &= 2\lambda \eta \Psi w w^T
\end{aligned} \tag{11}$$

We could absorb the 2 factor in this equation into  $\lambda$  to produce the dynamics:

$$\begin{aligned}
\frac{\partial \Psi}{\partial t} &= \lambda \eta \Psi w w^T \\
\frac{\partial w}{\partial t} &= -\eta \frac{\partial w}{\partial \theta} \Psi^T \Psi w
\end{aligned} \tag{12}$$

At a first look, this model adds an interesting layer of complexity over fixed tangent kernel learning: the kernel evolves in predictable and alignment-boosting ways. However, there's no strong empirical evidence that OFE captures any variant of GD training.

## C.2 Generalised Optimal Feature Evolution and GD training

To better capture GD/SGD/NGD dynamics, we first introduce the paradigm of Generalised Optimal Feature Evolution (GOFE):

$$\begin{aligned}
\frac{\partial \Psi}{\partial t} &= \eta \mathbf{V} \Psi w w^T \\
\frac{\partial w}{\partial t} &= -\eta \frac{\partial w}{\partial F} \Psi^T \mathbf{A} \Psi w = -\eta \frac{\partial^2 \mathcal{L}}{\partial F^2} \Psi^T \mathbf{A} \Psi w
\end{aligned} \tag{13}$$

where  $\mathbf{V}$  is a velocity vector that may or may not depend on time step  $t$ ,  $\mathbf{A}$  is a time-dependent matrix describing the training procedure used (i.e. for full batch GD,  $\mathbf{A}$  is simply the identity matrix, and for natural gradient descent,  $\mathbf{A}$  is the inverse of Fisher Information Matrix).  $\frac{\partial w}{\partial F}$  gradient of  $w$  w.r.t to the output  $F$ . The last equality is due to definition of  $w^T = \frac{\partial \mathcal{L}}{\partial F}$ . Note that in OFE,  $\mathbf{V}$  is simply a diagonal matrix with diagonal entries  $\lambda$ . Note that in practice the feature evolution is realised by the set of difference equations:

$$\begin{aligned}
\Delta_t(\Psi) &= \eta \mathbf{V}_t \Psi_t w_t w_t^T \\
\Delta_t(\theta) &= -\eta \mathbf{A}_t \Psi_t w_t
\end{aligned} \tag{14}$$

This would allow us to conduct several calculations exactly in the following. The  $t$  index each time step.

It turns out that for each gradient descent dynamics, be it full batch or stochastic GD or natural gradient descent, there is an equivalent formulation of its training dynamics in terms of GOFE. By 'equivalent' we mean that at each time step, the gradient propagated to the weights of the network is the same. To achieve this equivalence we need the following two dynamics of gradient changes to be the same:

Under GOFE:

$$\begin{aligned}\frac{\partial(\Psi w)}{\partial t} &= \frac{\partial(\Psi)}{\partial t}w + \Psi \frac{\partial(w)}{\partial t} \\ &= \eta \mathbf{V} \Psi w w^T w - \eta \Psi \frac{\partial^2 \mathcal{L}}{\partial F^2} \Psi^T \mathbf{A} \Psi w \\ &= \eta \|w\|^2 \mathbf{V} \Psi w - \eta \Psi \frac{\partial^2 \mathcal{L}}{\partial F^2} \Psi^T \mathbf{A} \Psi w\end{aligned}\quad (15)$$

Under gradient descent with gradient adjustment matrix  $\mathbf{A}$ :

$$\begin{aligned}\frac{\partial(\Psi w)}{\partial t} &= \frac{\partial(\Psi w)}{\partial \theta} \frac{\partial \theta}{\partial t} = \frac{\partial^2 \mathcal{L}}{\partial \theta^2} (-\eta \mathbf{A} \Psi w) = -\eta \frac{\partial^2 \mathcal{L}}{\partial \theta^2} \mathbf{A} \Psi w \\ &= -\eta \mathbf{H}_w \mathbf{A} \Psi w - \eta \Psi \frac{\partial^2 \mathcal{L}}{\partial F^2} \Psi^T \mathbf{A} \Psi w\end{aligned}\quad (16)$$

During the derivation we have used a well known decomposition of the loss hessian:

$$\frac{\partial^2 \mathcal{L}}{\partial \theta^2} = \mathbf{H}_w + \Psi \frac{\partial^2 \mathcal{L}}{\partial F^2} \Psi^T \quad (17)$$

where  $\mathbf{H}_w$  is the same as  $\mathbf{H}_w$  in Section 4. Equating the two dynamics we need:

$$\begin{aligned}\eta \|w\|^2 \mathbf{V} \Psi w - \eta \Psi \frac{\partial^2 \mathcal{L}}{\partial F^2} \Psi^T \mathbf{A} \Psi w &= -\eta \mathbf{H}_w \mathbf{A} \Psi w - \eta \Psi \frac{\partial^2 \mathcal{L}}{\partial F^2} \Psi^T \mathbf{A} \Psi w \\ \iff (\|w\|^2 \mathbf{V} + \mathbf{H}_w \mathbf{A}) \Psi w &= 0\end{aligned}\quad (18)$$

We hence set  $\mathbf{V} = -\frac{\mathbf{H}_w \mathbf{A}}{\|w\|^2}$ . Under the assumption that  $w$  and  $y$  are highly correlated at early training, we could directly derive the evolution of  $\Psi$ . In fact, under GD ( $\mathbf{A}$  being identity matrix):

$$\frac{\partial \Psi}{\partial t} = -\eta \frac{\mathbf{H}_w \mathbf{A}}{\|w\|^2} \Psi w w^T = -\eta \mathbf{H}_w \Psi \frac{w w^T}{\|w\|^2} = -\eta \mathbf{H}_w \Psi \frac{y y^T}{\|y\|^2} \quad (19)$$

We could test GOFE against results derived without it, in fact multiplying  $y$  to the above equation yields:

$$\frac{\partial \Psi y}{\partial t} = -\eta \mathbf{H}_w \Psi \frac{y y^T}{\|y\|^2} y = -\eta \mathbf{H}_w \Psi y \quad (20)$$

which is the continuous version of Eq. (8). Also for any fixed vector  $u$  orthogonal to  $y$ , we have:

$$\frac{\partial \Psi u}{\partial t} = -\eta \mathbf{H}_w \Psi \frac{y y^T}{\|y\|^2} u = 0 \quad (21)$$

This relates to the increase in tangent kernel anisotropy in [Baratin et al. \(2021\)](#), as  $u^T \Psi^T \Psi u$  stays constant over training while  $y^T \Psi^T \Psi y$  increases sharply due to large negative eigenvalues in  $\mathbf{H}_w$ .

### C.3 Explaining the Hierarchy using feature evolution scheme

Eq. (20) gives us a way to describe a way to describe  $\Psi(t+1)y$  as  $\mathbf{H}(t)\Psi(t)y$  for some matrix  $\mathbf{H}(t) = (\mathbf{I} - \eta\mathbf{H}_w(t))$  which also describes evolution of parameters. Take an orthogonal basis consisting of  $u_0 = \frac{y}{\|y\|}$ ,  $u_1 = \frac{1}{\sqrt{kN}}(1, 1, \dots, 1)^T$ ,  $u_2, \dots, u_N \in \mathbb{R}^{kN}$ ,  $\mathbf{U}$  be the  $kN \times kN$  matrix with  $u_i$  as columns and we would have:

$$\begin{aligned}
A_l(t+1) &= \frac{y^T \Psi(t+1)^T \mathbf{M}_l \Psi(t+1) y}{\|\Psi(t+1)^T \mathbf{M}_l \Psi(t+1) \mathbf{C}\|_F \|y\|^2} \\
&= A_l(t) \cdot \frac{u_0^T \Psi(t+1)^T \mathbf{M}_l \Psi(t+1) u_0}{u_0^T \Psi(t)^T \mathbf{M}_l \Psi(t) u_0} \cdot \frac{\|\mathbf{U}^T \Psi(t)^T \mathbf{M}_l \Psi(t) \mathbf{C} \mathbf{U}\|_F}{\|\mathbf{U}^T \Psi(t+1)^T \mathbf{M}_l \Psi(t+1) \mathbf{C} \mathbf{U}\|_F} \\
&\approx A_l(t) \cdot \frac{u_0^T \Psi(t)^T \mathbf{H}(t)^T \mathbf{M}_l \mathbf{H}(t) \Psi(t) u_0}{u_0^T \Psi(t)^T \mathbf{M}_l \Psi(t) u_0} \\
&= A_l(t) \cdot \frac{\theta(t)^T \mathbf{H}_y(t)^T \mathbf{H}^T \mathbf{M}_l \mathbf{H} \mathbf{H}_y(t) \theta(t)}{\theta(t)^T \mathbf{H}_y(t)^T \mathbf{M}_l \mathbf{H}_y(t) \theta(t)} \tag{22} \\
&\approx A_l(t) \cdot \frac{\text{tr}(\mathbf{H}_y(t)^T \mathbf{H}(t)^T \mathbf{M}_l \mathbf{H}(t) \mathbf{H}_y(t))}{\text{tr}(\mathbf{H}_y(t)^T \mathbf{M}_l \mathbf{H}_y(t))} \\
&\approx A_l(t) \cdot \frac{\text{tr}(\mathbf{M}_l (\mathbf{I} - \eta\mathbf{H}_w(t)) \mathbf{H}_w^2(t) (\mathbf{I} - \eta\mathbf{H}_w(t)))}{\text{tr}(\mathbf{M}_l \mathbf{H}_w^2(t))} \\
&= A_l(t) - 2\eta \frac{\text{tr}(\mathbf{M}_l \mathbf{H}_w^3(t))}{\text{tr}(\mathbf{M}_l \mathbf{H}_w^2(t))} + \eta^2 \frac{\text{tr}(\mathbf{M}_l \mathbf{H}_w^4(t))}{\text{tr}(\mathbf{M}_l \mathbf{H}_w^2(t))}
\end{aligned}$$

The first approximation holds in the case of large  $N$  and the second approximation is based on the assumption that  $\theta(t)$  is independent from  $\mathbf{H}_y(t)$  and  $\mathbf{H}(t)$ , and each entry is drawn from i.i.d normal distribution. The second approximation has its roots in Gradient Independence Appendix A.2. The third approximation uses Approximation 2. This derivation illustrates that hierarchical structure of CKA likely arise out of bias in  $\mathbf{H}_w$ 's third and fourth moment. Actually, for common learning rates of  $\approx 0.005$  used for deep networks,  $\mathbf{H}_w$ 's largest positive eigenvalue is usually around 5 – 15, hence the third part of Eq. (22) is dominated by the first and second part which is around 0.01 – 0.07. We later empirically illustrate interesting structural bias in  $\mathbf{H}_w(t)$ . Let  $\mathbf{V}(t)$  diagonalises  $\mathbf{H}_w(t)$ :

$$\begin{aligned}
\frac{\text{tr}(\mathbf{M}_l \mathbf{H}_w^3(t))}{\text{tr}(\mathbf{M}_l \mathbf{H}_w^2(t))} &= \frac{\text{tr}(\mathbf{V}(t)^T \mathbf{M}_l \mathbf{V}(t) \mathbf{V}(t)^T \mathbf{H}_w^3(t) \mathbf{V}(t))}{\text{tr}(\mathbf{V}(t)^T \mathbf{M}_l \mathbf{V}(t) \mathbf{V}(t)^T \mathbf{H}_w^2(t) \mathbf{V}(t))} \\
&= \frac{\sum_i c_i(t) \lambda_i^3}{\sum_i c_i(t) \lambda_i^2}
\end{aligned}$$

where  $c_i(t) := v_i(t)^T \mathbf{M}_l v_i(t)$  and  $\lambda_i(t)$  is the eigenvalue corresponding to  $v_i(t)$ . The quantity is a weighted average of all eigenvalues of  $\mathbf{H}_w(t)$ .

## Appendix D. Further experimental results

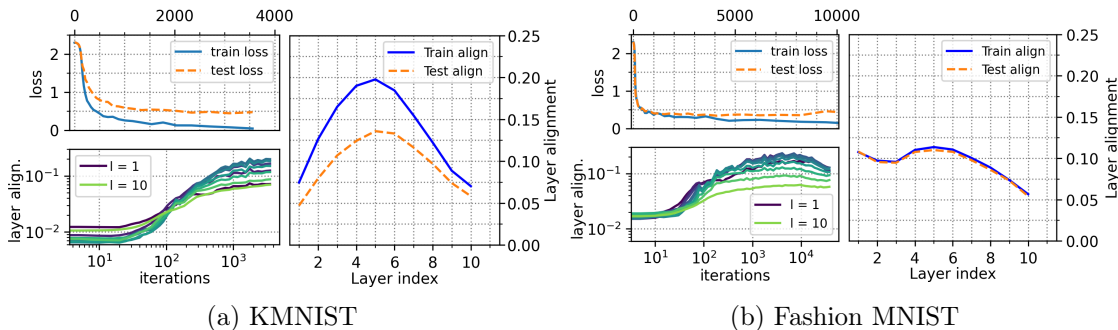


Figure 5: Supplementary experiments for Fig. 1. Layerwise alignment hierarchy for the KMNIST and Fashion MNIST datasets when trained on a FFNN with depth 10 and width 256. Left hand panels show progression of loss and layer alignment with iterations of SGD. Right hand panel shows layer alignment at the end of training.

Experiments in Figs. 1 and 5 used 10 layer FFNNs with 256 neurons in each layer, and were optimised with SGD with weight decay, momentum, and learning rates of 0.003.

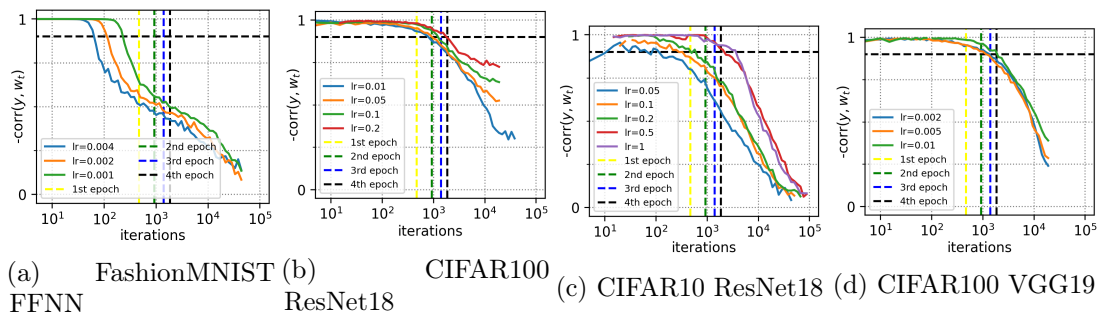


Figure 6: Further results from Fig. 3. Empirical validation of Approximation 1: a demonstration that  $-\text{corr}(\tilde{Y}, w_t) \approx 1$  at early  $t$ .

Details of experiments in Fig. 2: Feed forward Neural Network on CIFAR10, Fashion MNIST and MNIST using SGD optimizer with momentum and weight decay are included in Table 1, Table 2 and Table 3 resp. The learning rates are chosen as the one that produces best out of sample accuracy.

depth	width	learning rate	epochs	test accuracy
10	256	0.005	100	56%
20	256	0.003	100	58.3%
30	256	0.003	150	57.7%
40	256	0.001	200	58.7%
50	256	0.001	250	58%
60	256	0.0007	300	58.3%
70	256	0.0005	300	59.1%
80	256	0.0005	500	57.2%
90	256	0.0001	500	56.9%
100	256	0.0001	700	56%

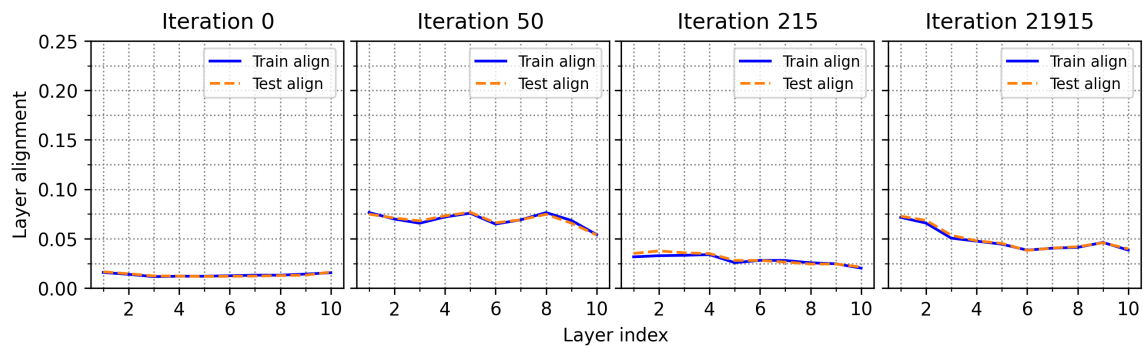
Table 1: CIFAR10 FFNN experiments to verify EH (Fig. 2c).

depth	width	learning rate	epochs	test accuracy
10	100	0.003	100	88.3%
20	100	0.004	100	88.6%
30	100	0.004	100	89.6%
40	100	0.002	100	88.9%
50	100	0.001	100	88.4%
60	100	0.0007	100	87.7%
70	100	0.0003	200	88.7%
80	100	0.0002	200	87.9%
90	100	0.0001	300	87.6%
100	100	$7 \times 10^{-5}$	300	88%

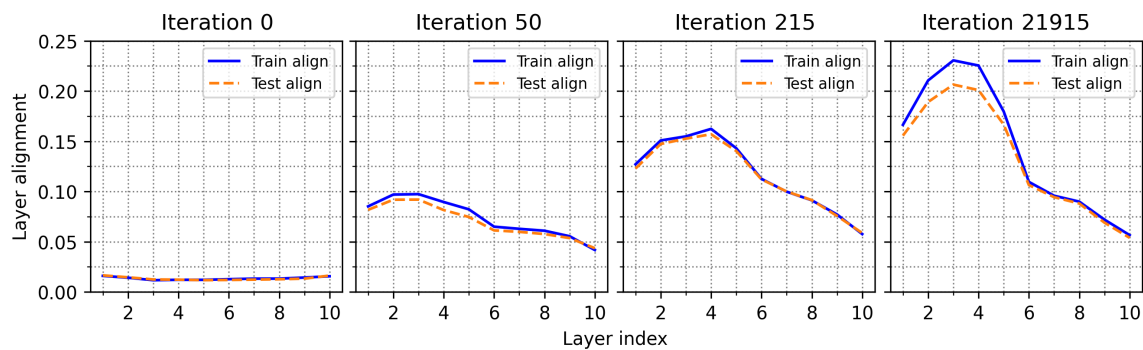
Table 2: FMNIST FFNN experiments to verify EH (Fig. 2b).

depth	width	learning rate	epochs	test accuracy
10	100	0.003	100	97%
20	100	0.003	100	97%
30	100	0.003	100	96.9%
40	100	0.002	100	97.6%
50	100	0.001	100	97.6%
60	100	0.0007	100	97.6%
70	100	0.0002	200	94.8%
80	100	0.0001	200	94.4%
90	100	0.0002	300	96.1%
100	100	0.0001	300	95.8%

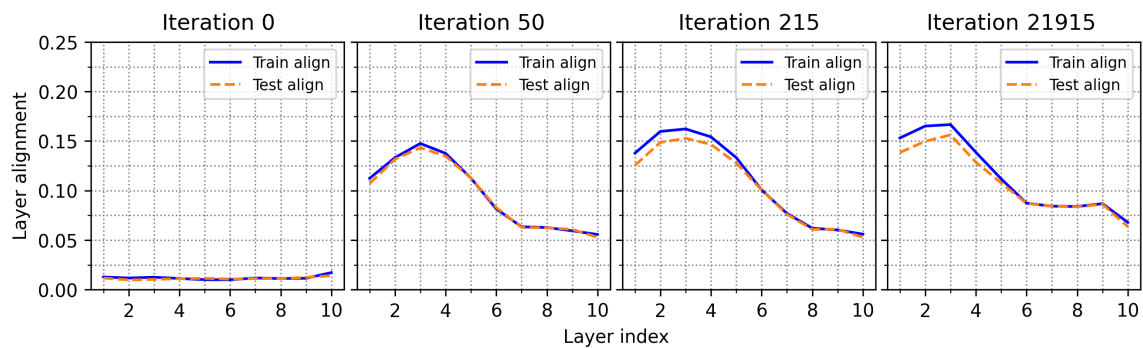
Table 3: MNIST FFNN experiments to verify EH (Fig. 2a).



(a) Learning Rate 0.0005, test accuracy 88.4%, test loss 0.53

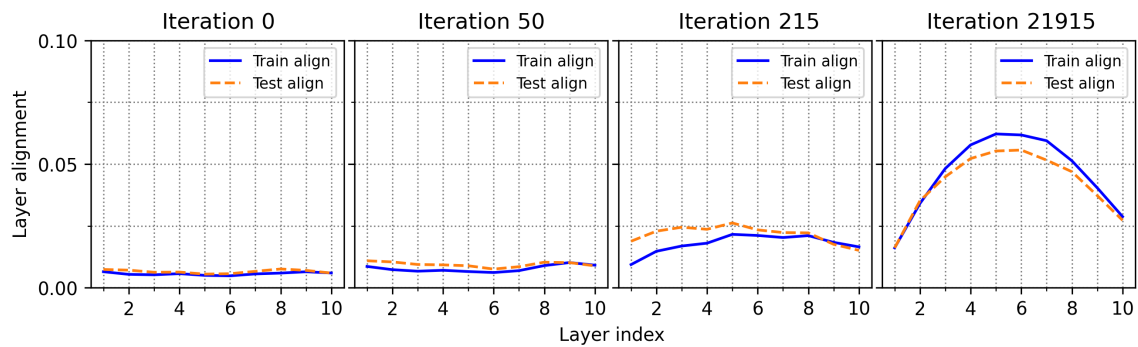


(b) Learning Rate 0.003, test accuracy 88.3%, test loss 0.53

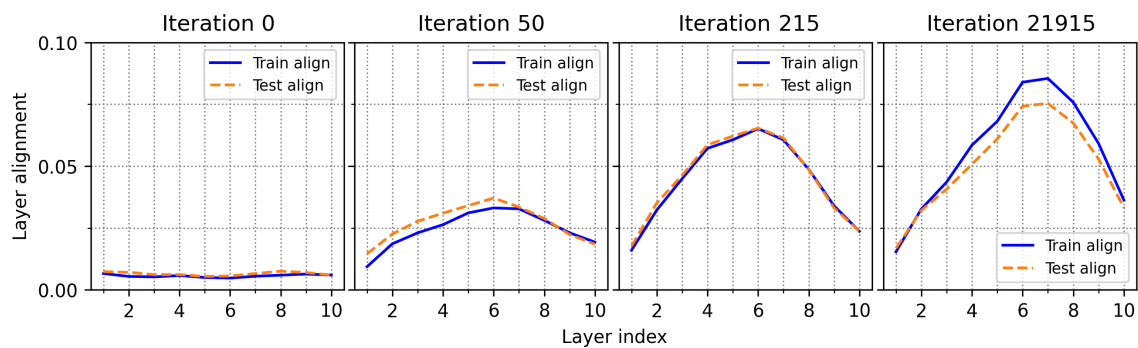


(c) Learning Rate 0.05, test accuracy 87.1%, test loss 0.41

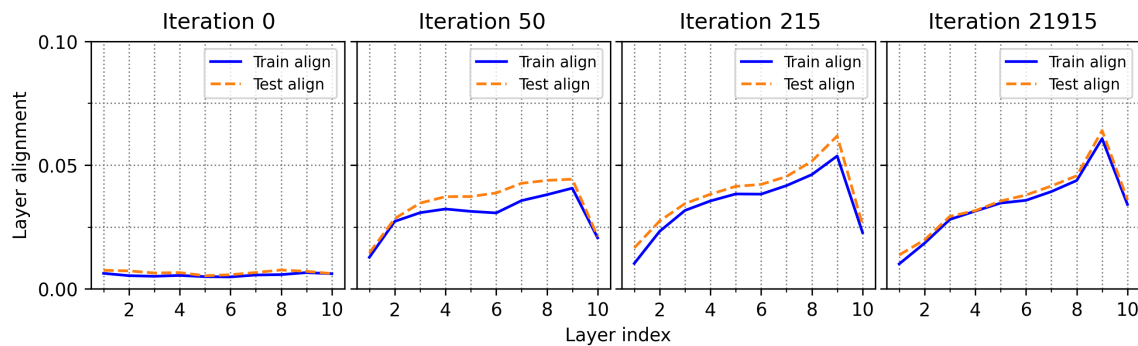
Figure 7: Alignment progress during training. Fashion MNIST. Further detail for Fig. 5b.



(a) Learning Rate 0.0005, test accuracy 53.9%, test loss 1.30



(b) Learning Rate 0.003, test accuracy 56.7%, test loss 1.21



(c) Learning Rate 0.05, test accuracy 51.4%, test loss 1.41

Figure 8: Alignment progress during training. CIFAR10. Further experiments from Fig. 1b.

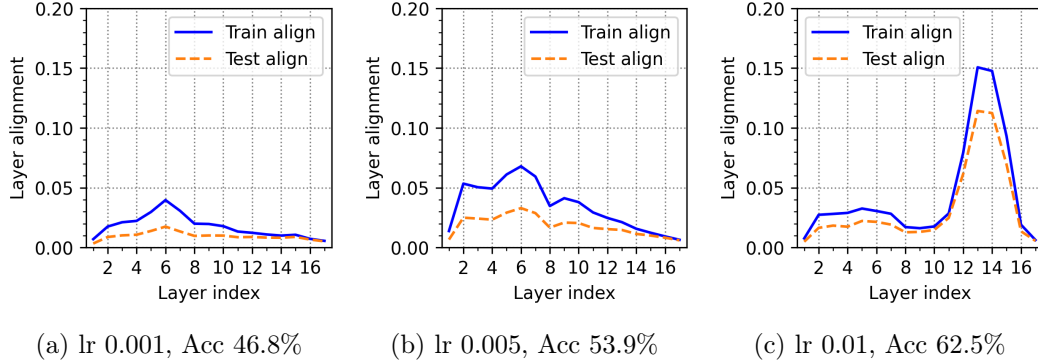


Figure 9: (a), (b) and (c) show VGG19 trained with SGD (with momentum and weight decay) for 100 epochs on CIFAR100 dataset with three different learning rates (lr). This is an addition to Fig. 4b with more complex architectures. To properly compare the three learning rates, training should be stopped at fixed training loss, as 100 epochs may not allow for convergence with the smaller learning rates (in (a) and (b)).

## Appendix E. Layer-wise alignment of the forward feature kernel

---

### Algorithm 1: Layer-wise maximisation of features

---

**input:** DNN  $N$  with  $L$  layers, LeakyReLU activations  $\phi$ , stochastic optimiser  $O$ , batch size  $b$ .

**input:** Training dataset  $S = \{(x_1, y_1), \dots, (x_n, y_n)\}$  and validation set  $V = \{(x_1, y_1), \dots, (x_{n'}, y_{n'})\}$  with normalised  $x_i$  (such that  $\|x_i\|^2 = 1$ ).

**for** layers  $l = 1, \dots, L - 1$  **do**

Normalise inputs to  $l$ , such that  $\|\phi(z_{l-1}(x))\|^2 = 1$ .

**while** True **do**

**for** Minibatches  $B$  in  $S$  **do**

With optimiser  $O$ , update weights and biases in layer  $l$  using loss function

$$L(B) = \sum_{x_i, x_j \in B} \|\vec{K}_l(x_i, x_j) - \frac{1}{2}\delta_{y_i, y_j}\|^2,$$

where  $\delta_{y_i, y_j} = 1$  if  $y_i = y_j$  else 0, and the unnormalised forward features,

$$\vec{K}_l(x_i, x_j) = \phi(z_{l-1}(x_i)) \cdot \phi(z_{l-1}(x_j)).$$

**end for**

End while based on increase/plateau of loss on the validation set,  $L(V)$ .

**end while**

Normalise layer  $l$ . Return  $\phi(z_l(x))$  as input for layer  $l + 1$

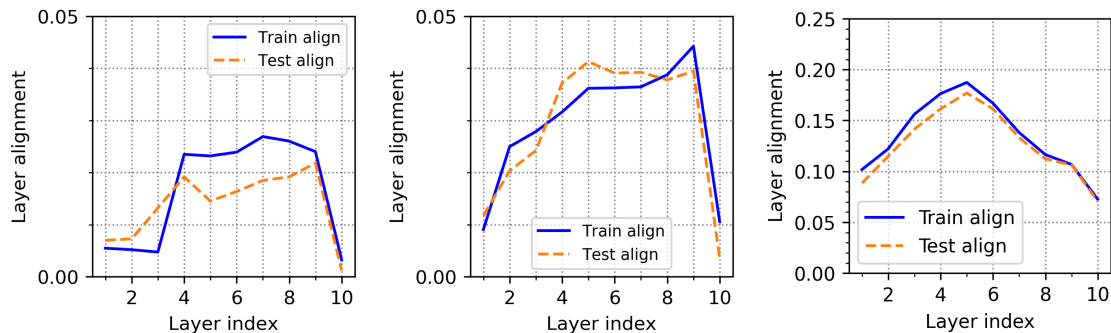
**end for**

Train layer  $L$  (the final classification layer) with optimiser  $O$  and cross entropy loss.

Return  $N$ .

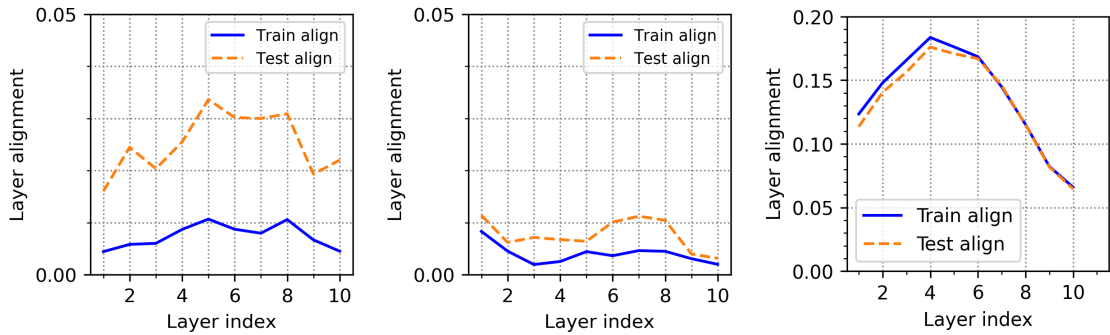
---

Previous work has studied layer-wise training of neural networks. Here, we adapt a method from Kulkarni and Karande (2017), which aims to maximise forward feature learning. Here, we confirm that our adapted method generalises well, and show the resulting layerwise CKA on CIFAR10 and MNIST (see Figs. 10 and 11). We will call the algorithm layer-wise feature maximisation (LFM) – see below. Finally, in Fig. 12, we show the layerwise CKA for networks with all but the last layer frozen during training. We find non-trivial CKA evolution, due to evolution of the backward feature kernel (despite trivial forward features).



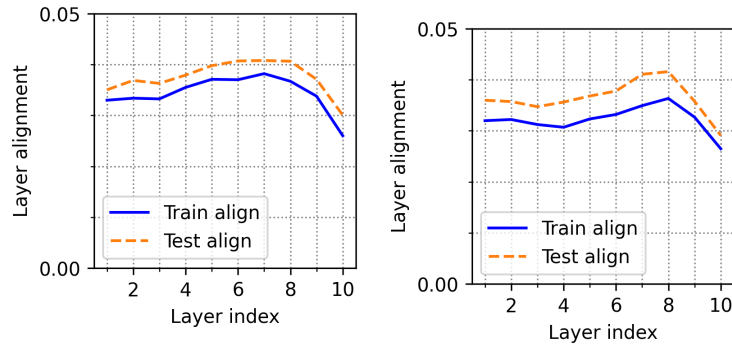
(a) LFM width 32. Acc 93.6% (b) LFM width 256. Acc 95.9% (c) width 32. Acc 96.9%

Figure 10: MNIST. (a) and (b) are trained with LFM (widths 32 and 256 respectively) with ADAM and a learning rate of 0.01, and (c) trained end-to-end with learning rate 0.003. (a) and (b) used a train/validation set split of 45000/5000, and (c) used 50000 training images with no validation set. The LFM does not produce a single peak in the same way an end-to-end trained network does (rather, several layers have approximately maximal alignment). The absolute magnitudes of alignment are also lower for the LFM – determining whether this is an artefact of the layer-wise normalisation scheme or otherwise is a topic of future work. Furthermore, as with experiments on CIFAR10 (Fig. 11), the LFM underperforms relative to the end-to-end neural network. More sophisticated early stopping schemes or different optimisers (Adam was used as other optimisers struggled to converge) may improve generalisation.



(a) LFM width 256. Acc 48.3% (b) LFM width 1024. Acc 49.2% (c) width 256. Acc 56.7%

Figure 11: CIFAR10. (a) and (b) are trained with LFM (widths 256 and 1024 respectively) with ADAM and a learning rate of 0.01, and (c) trained end-to-end with learning rate 0.003. (a) and (b) used a train/validation set split of 45000/5000, and (c) used 50000 training images with no validation set. The alignment for the LFM’s is very different to the end-to-end trained system, and the generalisation error is noticeably worse. Understanding why, or improving results is a topic of future work.



(a) Width 2048. Noise scale: 0.01 (b) Width 2048. Noise scale: 1.0

Figure 12: MNIST. All but the last layer is frozen during training (so no feature learning occurs). In the limit of infinite width, this is equivalent to sampling from an NNGP (Matthews et al., 2017). With 10 layers, 2048 is not sufficiently wide to obtain 100% training accuracy (see Table 4), but computing the CKA for each layer scales poorly with layer width. (a) and (b) achieve test accuracies of 91.9% and 88.1% respectively (due to comparatively small layer width). Noise scale determines the scale of the initialisation of the final layer – parameters are sampled i.i.d. from  $N(0, s^2 \times 2/L_w)$  (for noise scale  $s$ ), where  $L_w$  is the width of the layer. Decreasing the amount of noise in the last layer appears to shift the peak towards the center, although more careful study is required. Due to the frozen layers, no forward features are learned (so  $\vec{K}_l(x_i, x_j)$  is trivial), but evidently backward features  $\overleftarrow{K}_l(x_i, x_j)$  are non trivial. This is unlike neural networks trained end-to-end, which have both non-trivial forward and backward feature kernels.

Dataset	Number of layers	Width	Max train acc	Max test acc
MNIST	10	75000	97.6%	96.4%
MNIST	10	10000	96.4%	95.6%
MNIST	10	2048	92.6%	91.9%

Table 4: Best train/test accuracy for frozen neural networks as a function of layer widths. Network parameters are initialised i.i.d. from  $N(0, 2/L_w)$  where  $L_w$  is the width of the layer. Clearly, layers have to be very wide before near parity can be achieved with finite width unfrozen networks.